

NASA TECHNICAL NOTE



NASA TN D-7026

2.1

NASA TN D-7026

LOAN COPY: RETURN  
AFWL (DOGL)  
KIRTLAND AFB, N.



# DIGITAL COMPUTER PROGRAM FOR ANALYSIS OF CHUGGING INSTABILITIES

by *John R. Szuch*

*Lewis Research Center  
Cleveland, Ohio 44135*

NATIONAL AERONAUTICS AND SPACE ADMINISTRATION • WASHINGTON, D. C. • DECEMBER 1970





0133662

1. Report No. NASA TN D-7026	2. Government Accession No.	3. Recipient's Catalog No.	
4. Title and Subtitle DIGITAL COMPUTER PROGRAM FOR ANALYSIS OF CHUGGING INSTABILITIES		5. Report Date December 1970	
		6. Performing Organization Code	
7. Author(s) John R. Szuch		8. Performing Organization Report No. E-5629	
		10. Work Unit No. 128-31	
9. Performing Organization Name and Address Lewis Research Center National Aeronautics and Space Administration Cleveland, Ohio 44135		11. Contract or Grant No.	
		13. Type of Report and Period Covered Technical Note	
12. Sponsoring Agency Name and Address National Aeronautics and Space Administration Washington, D. C. 20546		14. Sponsoring Agency Code	
		15. Supplementary Notes	
16. Abstract A digital program, designed to generate chugging stability limits for bipropellant rocket engines, is described. The program computes combustion delays and other parameters required for solution of the characteristic equation. The equation is solved for critical values of the injector pressure drops and the chugging frequency. Stability limits are presented for a specified flox-methane engine system. Limits for throttling at constant mixture ratio and the effects of varying the injector geometry on stability are determined. Computer listings and typical printouts of results are presented.			
17. Key Words (Suggested by Author(s)) Chugging; Stability, instability; Digital, computer; Combustion; Dead time; Throttling; Injector; Rocket engines; Feed system; Dynamics; Vaporization, mixing; Impedance		18. Distribution Statement Unclassified - unlimited	
19. Security Classif. (of this report) Unclassified	20. Security Classif. (of this page) Unclassified	21. No. of Pages 77	22. Price* \$3.00

# DIGITAL COMPUTER PROGRAM FOR ANALYSIS OF CHUGGING INSTABILITIES

by John R. Szuch

Lewis Research Center

## SUMMARY

A digital program, designed to generate chugging stability limits for bipropellant rocket engines, has been developed and is described herein. The program is written in FORTRAN IV language for use with the IBM 7094 computer. The program computes combustion delays, gas residence time, characteristic velocity, and other steady-state parameters required for solution of the characteristic equation. The characteristic equation is solved by the computer for critical values of the injector pressure drops and the chugging frequency. Stability limits have been generated for a specified flox-methane engine system. Results have been obtained for two injector configurations. For each injector configuration, limits for throttling at constant mixture ratio and the effects of varying the fuel injector area on stability were determined. Digital results were compared with available analog data to test the program. For both injector configurations, the predicted throttling limit was about 5 to 1 because of higher frequency (500 Hz) instabilities, characteristic of the chugging model. Typical computer listings and printouts of results are presented.

## INTRODUCTION

One of the problems often encountered in the development of liquid-propellant rocket engines is the occurrence of low-frequency instabilities, commonly referred to as chugging. Chugging is caused by a coupling of the propellant feed system with the combustion dynamics in such a way as to reinforce any disturbance in pressure or propellant flow.

Many analyses of chugging have shown that the controlling factors in determining low-frequency stability are the time delays associated with the atomization, vaporization, and combustion processes. Without these delays, the chamber-injector-feed system would be inherently stable.

The validity of a double-dead-time model (ref. 1) in analyzing chugging has been demonstrated in references 2 and 3. Previous analyses involved the use of a single-

dead-time model (ref. 4) with combustion delay, calculated for the propellant having the longer drop lifetime, applied to both propellants. The double-dead-time model requires the application to each propellant of its respective time delay and results in significantly different stability characteristics. Experimental data, reported in references 2, 3, and 5 to 7 have been matched using the double-dead-time model.

The implementation of chugging models has traditionally been done on the analog computer. However, as the models became more sophisticated and as engine configurations and propellant combinations changed, the need for a high-speed digital stability program became more evident.

A digital program, designed to generate stability limits for bipropellant rocket engines, has been developed and is described herein. The program was written in FORTRAN IV language for use with the IBM 7094 computer. Linearized feed-system impedances are evaluated by the program at each frequency of interest. In addition to chamber and injector flow dynamics, the program can handle combinations of pumps, valves, manifolds, and lines. For any selected engine configuration, the program computes the required steady-state engine parameters for solution of the characteristic equation. Available vaporization (ref. 8) and drop-size (ref. 9) correlations are used to calculate combustion delay times. The characteristic equation is solved by the computer for critical values of the injector pressure drops and the chugging frequency.

Stability limits have been generated for a specific flow (82.6 percent fluorine) - methane engine system. An expander cycle with a turbine-bypass throttle has been assumed. Results have been obtained for two candidate injector types. For each injector configuration, limits for throttling at constant mixture ratio and the effects of varying the fuel injection area on stability were determined using the digital program. Digital results were compared with available analog data to test the program and the linearization procedures.

Although the existing computer program is designed for the case of a completely vaporized fuel, the program is easily modified to handle liquid-liquid propellant combinations. The steps required for this modification, together with other aids to the user, are included in an appendix to this report.

## ANALYSIS

### Derivation of Characteristic Equation

The combustion process in a bipropellant rocket engine is still not clearly understood, although what takes place is qualitatively known. Figure 1 shows, schematically, the assumed model for a bipropellant rocket combustor. Initially, the propellants are

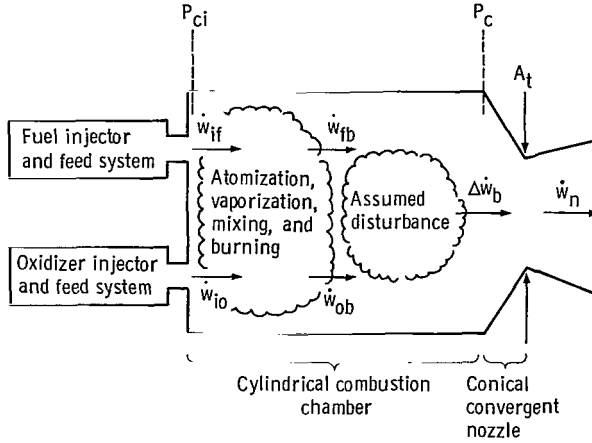


Figure 1. - Schematic of bipropellant combustor.

injected into the combustion chamber. The propellants then atomize, vaporize, and mix; they then react to produce hot gases. Their flow rates are determined by the conditions upstream and downstream of the injector element and the injector geometry. These processes are gradual and continuous. For mathematical expediency, however, they are treated in a discontinuous manner. A time interval between injection and a sudden conversion to vaporized propellant is assumed and referred to as the vaporization time delay  $\sigma_v$ . The time interval between the conversion to vaporized propellant and the conversion to burned gas is similarly referred to as the gas-phase mixing delay  $\sigma_m$ . For this analysis, the time delays are assumed to be invariant with time. With these assumptions, the following equations relate the rate of change of burned products to the injected propellant flow rates:

$$\dot{w}_{ob}(t) = \dot{w}_{io}(t - \bar{\sigma}_{vo} - \bar{\sigma}_m) \quad (1)$$

$$\dot{w}_{fb}(t) = \dot{w}_{if}(t - \bar{\sigma}_{vf} - \bar{\sigma}_m) \quad (2)$$

(All symbols are defined in appendix A.)

If the burned products behave as a perfect gas,

$$P_c(t) = \left( \frac{R_g T}{V} \right)_c W_c(t) \quad (3)$$

Assuming a small disturbance in the rate of change of burned products  $\Delta \dot{w}_b$  and using the conservation of mass yields

$$\frac{d}{dt} [W_c(t)] = \dot{w}_{ob}(t) + \dot{w}_{fb}(t) + \Delta \dot{w}_b(t) - \dot{w}_n(t) \quad (4)$$

For a choked nozzle,

$$\dot{w}_n(t) = \frac{P_c(t) A_t g_c}{c^*(t)} \quad (5)$$

Equations (1) to (5) can be combined to give the following equation relating total pressure at the nozzle throat to the injected propellant flow rates and the disturbance:

$$\frac{V_c}{A_t g_c} c^*(t) \frac{d}{dt} \left[ \frac{P_c(t)}{R_g T_c(t)} \right] + P_c(t) = \frac{c^*(t)}{A_t g_c} \left[ \dot{w}_{io}(t - \bar{\sigma}_{To}) + \dot{w}_{if}(t - \bar{\sigma}_{Tf}) + \Delta \dot{w}_b(t) \right] \quad (6)$$

where

$$\bar{\sigma}_{To} = \bar{\sigma}_{Vo} + \bar{\sigma}_m$$

$$\bar{\sigma}_{Tf} = \bar{\sigma}_{Vf} + \bar{\sigma}_m$$

Equation (6) is nonlinear and must be linearized to obtain the desired analytical solution. Equation (6) was linearized by assuming small perturbations in the system variables about a steady-state operating point and neglecting products of perturbations:

$$\frac{\bar{c}^*}{A_t g_c (\bar{R}_g \bar{T})_c} \frac{d\tilde{P}_c(t)}{dt} + \tilde{P}_c(t) = \frac{\bar{c}^*}{A_t g_c} \left[ \tilde{w}_{io}(t - \bar{\sigma}_{To}) + \tilde{w}_{if}(t - \bar{\sigma}_{Tf}) + \Delta \tilde{w}_b(t) \right] + \left( \frac{\bar{w}_o + \bar{w}_f}{A_t g_c} \right) \tilde{c}^*(t) + \frac{\bar{c}^*}{A_t g_c} \frac{\bar{P}_c}{(\bar{R}_g \bar{T})_c^2} \frac{d}{dt} (\widetilde{R_g T})_c(t) \quad (7)$$

The coefficient  $\bar{c}^*/[A_t g_c (\bar{R}_g \bar{T})_c]$  is the gas-residence time  $\bar{\theta}_g$  and is invariant with time. It is generally accepted that for small perturbations from steady state, the chamber temperature  $T_c$  remains nearly constant. Therefore, the last term on the right hand side of equation (7) was set equal to zero. Equation (7) is then rewritten as

$$\bar{\theta} \frac{d\tilde{P}_c(t)}{dt} + \tilde{P}_c(t) = \frac{\bar{c}^*}{A_t g_c} \left[ \tilde{w}_{io}(t - \bar{\sigma}_{To}) + \tilde{w}_{if}(t - \bar{\sigma}_{Tf}) + \Delta \dot{w}_b(t) \right] + \left( \frac{\bar{w}_o + \bar{w}_f}{A_t g_c} \right) \tilde{c}^*(t) \quad (8)$$

The theoretical characteristic velocity  $c_{th}^*$  is a known function of the chamber mixture ratio; that is,

$$c_{th}^*(t) = \mathcal{G} \left[ \frac{O}{F}(t) \right] \quad (9)$$

$$\frac{O}{F}(t) = \frac{\dot{w}_{io}(t - \bar{\sigma}_{To})}{\dot{w}_{if}(t - \bar{\sigma}_{Tf})} = \frac{\dot{w}_{ob}(t)}{\dot{w}_{fb}(t)} \quad (10)$$

Linearization of equations (9) and (10) yields the following equation relating perturbations in  $c_{th}^*$  to perturbations in the injected propellant flow rates:

$$\tilde{c}_{th}^* = \frac{1}{\bar{w}_f} \left[ \frac{\partial c_{th}^*}{\partial \left( \frac{O}{F} \right)} \right] \tilde{w}_{io}(t - \bar{\sigma}_{To}) - \frac{1}{\bar{w}_f} \left( \frac{\bar{O}}{\bar{F}} \right) \left[ \frac{\partial c_{th}^*}{\partial \left( \frac{O}{F} \right)} \right] \tilde{w}_{if}(t - \bar{\sigma}_{Tf}) \quad (11)$$

Assuming that the actual characteristic velocity  $c^*(t)$  is related to the theoretical value by a time-invariant efficiency,

$$c^*(t) = \bar{\eta}_{c^*} c_{th}^*(t) \quad (12)$$

equations (8), (11), and (12) can be combined to yield

$$\bar{\theta} \frac{d\tilde{P}_c(t)}{dt} + \tilde{P}_c(t) = \bar{X} \tilde{w}_{io}(t - \bar{\sigma}_{To}) + \bar{F} \tilde{w}_{if}(t - \bar{\sigma}_{Tf}) + \frac{\bar{c}^*}{A_t g_c} \Delta \dot{w}_b(t) \quad (13)$$

where

$$\bar{X} = \frac{\bar{\eta}_{c^*}}{A_t g_c} \left\{ \bar{c}_{th}^* + \left[ \left( \frac{\bar{O}}{\bar{F}} \right) + 1 \right] \left[ \frac{\partial \bar{c}_{th}^*}{\partial \left( \frac{\bar{O}}{\bar{F}} \right)} \right] \right\} \quad (14)$$

$$\bar{F} = \frac{\bar{\eta}_{c^*}}{A_t g_c} \left\{ \bar{c}_{th}^* - \left( \frac{\bar{O}}{\bar{F}} \right) \left[ \left( \frac{\bar{O}}{\bar{F}} \right) + 1 \right] \left[ \frac{\partial \bar{c}_{th}^*}{\partial \left( \frac{\bar{O}}{\bar{F}} \right)} \right] \right\} \quad (15)$$

The Laplace transform of equation (13) is

$$(\bar{\theta}_g s + 1) \tilde{P}_c(s) = \bar{X} \tilde{w}_{io}(s) e^{-\bar{\sigma}_{T_o} s} + \bar{F} \tilde{w}_{if}(s) e^{-\bar{\sigma}_{T_f} s} + \frac{\bar{c}^*}{A_t g_c} \Delta \dot{w}_b(s) \quad (16)$$

In general, the perturbations in the injected propellant flow rates can be related to the perturbations in the chamber pressure at the injector face  $P_{ci}$  by

$$\tilde{w}_{io}(s) = - \frac{1}{Z_{so}(s)} \tilde{P}_{ci}(s) \quad (17)$$

$$\tilde{w}_{if}(s) = - \frac{1}{Z_{sf}(s)} \tilde{P}_{ci}(s) \quad (18)$$

where  $Z_{so}(s)$  and  $Z_{sf}(s)$  are the linearized output impedances of the oxidizer and fuel feed systems, respectively. The impedances are evaluated at the injector face and include the impedances of the injector, valves, pumps, etc.

The chamber pressure at the injector face  $P_{ci}$  and the chamber pressure at the throat  $P_c$  can be related by considering the time rate of change of momentum of the flow between the injector and the nozzle inlet. By equating the pressure force and inertia force on the gas, one obtains

$$p_{ci} - p_c = \frac{\dot{w}_c}{A_c g_c} (v_c - v_{ci}) = \frac{v_{c^o}^2}{g_c} - \frac{v_{ci}^2}{g_c} \quad (19)$$

where  $p_{ci}$  and  $p_c$  are the static chamber pressures at the injector face and nozzle inlet, respectively. Equation (19) may be written in terms of the Mach number such that

$$\frac{p_{ci}}{p_c} = \frac{1 + \bar{\gamma}_c \bar{M}_c^2}{1 + \bar{\gamma}_c \bar{M}_{ci}^2} \quad (20)$$

By definition, the total pressures  $P_c$  and  $P_{ci}$  are related to the static pressures  $p_c$  and  $p_{ci}$ , respectively, by

$$P_c = p_c \left[ 1 + \left( \frac{\bar{\gamma}_c - 1}{2} \right) \bar{M}_c^2 \right]^{\bar{\gamma}_c / (\bar{\gamma}_c - 1)} \quad (21)$$

$$P_{ci} = p_{ci} \left[ 1 + \left( \frac{\bar{\gamma}_c - 1}{2} \right) \bar{M}_{ci}^2 \right]^{\bar{\gamma}_c / (\bar{\gamma}_c - 1)} \quad (22)$$

Combining equations (20), (21), and (22) and assuming that  $M_{ci}$  is small (large chamber) results in

$$\frac{P_{ci}}{P_c} = \frac{1 + \bar{\gamma}_c \bar{M}_c^2}{\left[ 1 + \left( \frac{\bar{\gamma}_c - 1}{2} \right) \bar{M}_c^2 \right]^{\bar{\gamma}_c / (\bar{\gamma}_c - 1)}} = \bar{K}_c \quad (23)$$

By assuming that the pressure ratio  $\bar{K}_c$  is time-invariant and that there is no total pressure loss in the converging section of the nozzle, equations (16), (17), (18), and (23) may be combined to yield the following transfer function:

$$\frac{\tilde{P}_c(s)}{\Delta \dot{w}_b(s)} = \frac{\frac{\bar{c}^*}{A_t g_c}}{\bar{\theta}_g s + 1 + \frac{\bar{X} \bar{K}_c}{Z_{so}(s)} e^{-\bar{\sigma}_{To} s} + \frac{\bar{F} \bar{K}_c}{Z_{sf}(s)} e^{-\bar{\sigma}_{Tf} s}} \quad (24)$$

The transfer function describes the response of the total pressure at the nozzle inlet  $P_c$  to the disturbance in the rate of change in burned products  $\Delta \dot{w}_b$ .

The characteristic equation, describing the stability of the bipropellant system, is obtained by setting the denominator of equation (24) equal to zero. The result is

$$-1 = \frac{\frac{\overline{XK}_c}{Z_{so}(S)} e^{-\overline{\sigma}_{T_o} S} + \frac{\overline{FK}_c}{Z_{sf}(S)} e^{-\overline{\sigma}_{T_f} S}}{\overline{\theta}_g S + 1} \quad (25)$$

It can be shown that equation (25) applies regardless of where the disturbance is introduced into the system.

Figure 2 is a block diagram of the linearized bipropellant system described by equation (25).

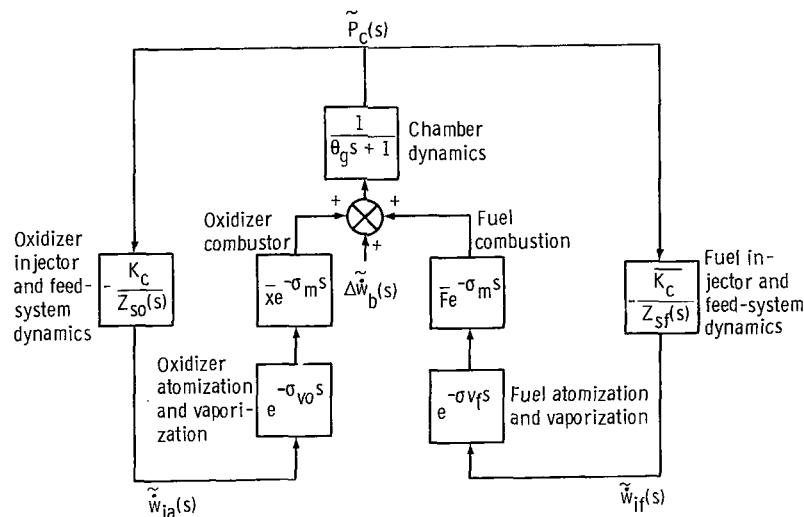


Figure 2. - Block diagram of chugging model for general bipropellant engine system.

tion (25). If all of the roots of equation (25) have negative real parts ( $S = \lambda + j\omega$ ,  $\lambda < 0$ ) the system is stable. The first appearance of a root on the imaginary axis ( $S = j\omega$ ) defines the boundary of stability.

### Solution of Characteristic Equation

By separating the impedances  $Z_{so}$  and  $Z_{sf}$  into their respective real and imagi-

nary parts and letting  $S = j\omega$ , the characteristic equation (eq. (25)) can be separated to give

$$-1 = \frac{\overline{XK}_c \mathcal{A}_o \cos(\omega \bar{\sigma}_{T_o}) - \overline{XK}_c \mathcal{J}_o \sin(\omega \bar{\sigma}_{T_o})}{\mathcal{A}_o^2 + \mathcal{J}_o^2} + \frac{\overline{FK}_c \mathcal{A}_f \cos(\omega \bar{\sigma}_{T_f}) - \overline{FK}_c \mathcal{J}_f \sin(\omega \bar{\sigma}_{T_f})}{\mathcal{A}_f^2 + \mathcal{J}_f^2} \quad (26)$$

$$\omega \bar{\theta}_g = \frac{\overline{XK}_c \mathcal{J}_o \cos(\omega \bar{\sigma}_{T_o}) + \overline{XK}_c \mathcal{A}_o \sin(\omega \bar{\sigma}_{T_o})}{\mathcal{A}_o^2 + \mathcal{J}_o^2} + \frac{\overline{FK}_c \mathcal{J}_f \cos(\omega \bar{\sigma}_{T_f}) + \overline{FK}_c \mathcal{A}_f \sin(\omega \bar{\sigma}_{T_f})}{\mathcal{A}_f^2 + \mathcal{J}_f^2} \quad (27)$$

where

$$\mathcal{A}_o + j \mathcal{J}_o = Z_{so}(j\omega)$$

$$\mathcal{A}_f + j \mathcal{J}_f = Z_{sf}(j\omega)$$

Specifying angular frequency  $\omega$  allows equations (26) and (27) to be solved for two selected critical parameters. The real parts  $\mathcal{A}_o$  and  $\mathcal{A}_f$  were selected because they could be related to the injector flow resistances  $\frac{d \Delta P}{d \dot{w}}$  which are independent of frequency. Specification of a parameter other than frequency requires the iterative solution of transcendental equations involving frequency.

Appendix B outlines the steps required to solve equations (26) and (27). The procedure followed results in the following quadratic equations relating the critical value of the real part of the oxidizer impedance  $\mathcal{A}'_o(\omega')$  to the imaginary parts of the feed system impedances  $\overline{\mathcal{J}}_o(\omega')$  and  $\overline{\mathcal{J}}_f(\omega')$  (the engine gains, delay times, imaginary parts, etc., are evaluated at the selected operating point):

$$\begin{aligned} & \mathcal{A}'_o{}^2 \left[ Y - \frac{\overline{\mathcal{J}}_f}{\overline{FK}_c} \left( 1 + \omega'^2 \bar{\theta}_g^2 \right) \right] + \mathcal{A}'_o \left\{ -\overline{XK}_c \sin(\omega' \bar{\sigma}_{T_o} - \omega' \bar{\sigma}_{T_f}) - \frac{2\overline{X}\overline{\mathcal{J}}_f}{\overline{F}} \right. \\ & \times \left[ \cos(\omega' \bar{\sigma}_{T_o}) - \omega' \bar{\theta}_g \sin(\omega' \bar{\sigma}_{T_o}) \right] \left. \right\} + \left\{ \overline{\mathcal{J}}_o{}^2 Y - \overline{\mathcal{J}}_o \overline{XK}_c \cos(\omega' \bar{\sigma}_{T_o} - \bar{\sigma}_{T_f}) \right. \\ & \left. + \frac{2\overline{X}\overline{\mathcal{J}}_o \overline{\mathcal{J}}_f}{\overline{F}} \left[ \sin(\omega' \bar{\sigma}_{T_o}) + \omega' \bar{\theta}_g \cos(\omega' \bar{\sigma}_{T_o}) \right] - \frac{\overline{\mathcal{J}}_f \overline{\mathcal{J}}_o^2}{\overline{FK}_c} \left( 1 + \omega'^2 \bar{\theta}_g^2 \right) - \frac{\overline{\mathcal{J}}_f \overline{X}^2 \overline{K}_c}{\overline{F}} \right\} = 0 \quad (28) \end{aligned}$$

where

$$Y = \omega' \bar{\theta}_g \cos(\omega' \bar{\sigma}_{Tf}) + \sin(\omega' \bar{\sigma}_{Tf})$$

The solution of equation (28) is used to compute the corresponding critical value of the real part of the fuel impedance  $\mathcal{A}'_f$ . The equation, which is derived in appendix B, is

$$\frac{1}{\mathcal{A}'_f} = \frac{\mathcal{A}'_o \omega' \bar{\theta}_g + \bar{\mathcal{J}}_o - \bar{X} \bar{K}_c \sin(\omega' \bar{\sigma}_{T_o})}{\bar{F} \bar{K}_c \mathcal{A}'_o \sin(\omega' \bar{\sigma}_{Tf}) - \bar{F} \bar{\mathcal{J}}_o \bar{K}_c \cos(\omega' \bar{\sigma}_{Tf}) - \bar{X} \bar{K}_c \bar{\mathcal{J}}_f \cos(\omega' \bar{\sigma}_{T_o}) + \omega' \bar{\theta}_g \bar{\mathcal{J}}_o \bar{\mathcal{J}}_f - \bar{\mathcal{J}}_f \mathcal{A}'_o} \quad (29)$$

The values of  $\mathcal{A}'_o$  and  $\mathcal{A}'_f$ , which satisfy equations (28) and (29) at frequency  $\omega'$ , must be related to the physical injector and feed systems being studied. In addition, the imaginary parts  $\bar{\mathcal{J}}_o$  and  $\bar{\mathcal{J}}_f$  must be computed for the particular feed system and operating point at each frequency before solving equations (28) and (29). The discussion of how this is done is contained in the next section.

## Evaluation of System Parameters

The primary function of the computer program is to test the stability of a specified engine configuration operating at a selected thrust level or chamber pressure  $P_c$ . The program may be used to study the effects on stability of changing the engine geometry at fixed thrust, throttling the engine with fixed geometry, or combinations of both. Regardless of the type of study, solutions of equations (28) and (29) to find the critical feed system impedances  $\mathcal{A}'_o$  and  $\mathcal{A}'_f$  require prior calculations of the system parameters at the specified operating point. These calculations are carried out by the computer program.

Engine gains. - The oxidizer and fuel gains  $\bar{X}$  and  $\bar{F}$ , respectively, are computed using equations (14) and (15). A curve of the theoretical  $c^*$  against mixture ratio for the specified propellant combination is required. For this study, equilibrium properties are used with the propellant temperatures equal to full thrust values. Although a dynamic sensitivity of  $c^*_{th}$  to only mixture ratio is assumed, a static sensitivity to both mixture ratio and chamber pressure is used to determine the steady-state value of  $\bar{c}^*_{th}$ . The digital program computes both  $\bar{c}^*_{th}$  and  $\frac{\partial \bar{c}^*_{th}}{\partial (\bar{O}/\bar{F})}$  for known values of  $\bar{P}_c$  and  $\bar{O}/\bar{F}$ . Required input information also includes the throat area  $A_t$  and combustion efficiency

$\bar{\eta}_{c^*}$ . The parameter  $\bar{\eta}_{c^*}$  is computed at each operating condition and a discussion of the calculation follows.

The chamber momentum loss parameter  $\bar{K}_c$  is calculated using equation (23). The specific heat ratio  $\bar{\gamma}_c$  is determined from specified values of  $\bar{P}_c$  and  $\bar{O}/\bar{F}$ . The Mach number at the nozzle entrance  $\bar{M}_c$  is calculated from

$$\bar{M}_c = \frac{1}{\epsilon_c} \left( \frac{2}{\bar{\gamma}_c + 1} \right)^{(\bar{\gamma}_c + 1)/2(\bar{\gamma}_c - 1)} \quad (30)$$

where  $\epsilon_c$  is the nozzle contraction ratio or  $A_c/A_t$ .

Combustion efficiency. - The combustion efficiency  $\bar{\eta}_{c^*}$  is a measure of the degree of mixing and vaporization of the propellants within the chamber and nozzle. Work described in reference 8 was directed at relating the efficiency due to incomplete vaporization  $\bar{\eta}_{\text{vap}}$  to the chamber geometry and operating conditions. For that study, perfect mixing of propellants was assumed. It is here assumed that

$$\bar{\eta}_{c^*} = \bar{\eta}_{\text{vap}} \bar{\eta}_{\text{mix}} \quad (31)$$

The following equations were derived in reference 8 to compute  $\bar{\eta}_{\text{vap}}$ :

$$\bar{\eta}_{\text{vap}} = \frac{\mathcal{G} \left[ \frac{\mathcal{O}(\bar{O})}{\mathcal{F}(\bar{F})} \right]}{\mathcal{G} \left( \frac{\bar{O}}{\bar{F}} \right)} \frac{\mathcal{O} \bar{w}_o + \mathcal{F} \bar{w}_f}{\bar{w}_o + \bar{w}_f} \quad (32)$$

where

$\mathcal{O}$  fraction of oxidizer mass vaporized within chamber nozzle; function of  $l_{\text{gen}, o}$

$\mathcal{F}$  fraction of fuel mass vaporized within chamber nozzle; function of  $l_{\text{gen}, f}$

$\mathcal{G}$  functional relation of  $c_{\text{th}}^*$  and mixture ratio

and where  $l_{\text{gen}}$  is a generalized length parameter

$$\bar{l}_{\text{gen, o}} = \left( \frac{l_c}{\epsilon_c^{0.44}} + \frac{0.83 l_n}{\epsilon_c^{0.22} \rho^{0.33}} \right) \frac{\left( \frac{\bar{P}_c}{2.07 \times 10^6} \right)^{0.66}}{\left( 1 - \frac{\bar{T}_o}{T_{\text{cr, o}}} \right)^{0.4} \left( \frac{\bar{r}_o}{7.62 \times 10^{-5}} \right)^{1.45} \left( \frac{\bar{v}_o}{30.5} \right)^{0.75} \left( \frac{\mathcal{M}_o}{100} \right)^{0.35} \left( \frac{H_o}{3.26 \times 10^5} \right)^{0.8}} \quad (33)$$

$$\bar{l}_{\text{gen, f}} = \left( \frac{l_c}{\epsilon_c^{0.44}} + \frac{0.83 l_n}{\epsilon_c^{0.22} \rho^{0.33}} \right) \frac{\left( \frac{\bar{P}_c}{2.07 \times 10^6} \right)^{0.66}}{\left( 1 - \frac{\bar{T}_f}{T_{\text{cr, f}}} \right)^{0.4} \left( \frac{\bar{r}_f}{7.62 \times 10^{-5}} \right)^{1.45} \left( \frac{\bar{v}_f}{30.5} \right)^{0.75} \left( \frac{\mathcal{M}_f}{100} \right)^{0.35} \left( \frac{H_f}{3.26 \times 10^5} \right)^{0.8}} \quad (34)$$

Calculation of the generalized length parameter for each propellant requires knowledge of the propellant drop radius  $\bar{r}$ . For liquid-liquid systems, the drop radii are usually assumed to be only functions of the injection element sizes (ref. 8). Experimental data presented in reference 9 for concentric tube injectors with gaseous fuel injected through the annuli indicated that the mean oxidizer drop radius  $\bar{r}_o$  is also proportional to the square-root of the injection momentum ratio; that is,

$$\bar{r}_o = K_r d_o \left( \frac{\bar{w}_o \bar{v}_o}{\bar{w}_f \bar{v}_f} \right)^{0.5} \quad (35)$$

(concentric-tube injector, gaseous-fuel).

Using experimental data presented in references 2, 3, 5, and 7, a proportionality constant  $K_r$  of 0.118 was calculated for liquid-oxygen droplets. However, references 8 and 10 indicate the following effect of propellant properties on drop size:

$$\bar{r} \propto \left( \frac{\mu \delta}{\rho} \right)^{0.25} \quad (36)$$

where

- $\mu$  viscosity of liquid
- $\delta$  surface tension of liquid
- $\rho$  density of liquid

To compute the drop radius for propellants other than liquid oxygen, the experimentally determined proportionality constant ( $K_r = 0.118$ ) must be modified to include the effect described by equation (36). The resultant expression for the drop radius of any liquid oxidizer droplet, injected through a concentric element with gaseous fuel injected through the annulus, is

$$\bar{r}_o = 0.118 d_o \left( \frac{\delta_o \mu_o \rho_o, 2}{\delta_o, 2 \mu_o, 2 \rho_o} \right)^{0.25} \left( \frac{\bar{w}_o \bar{v}_o}{\bar{w}_f \bar{v}_f} \right)^{0.5} \quad (37)$$

For this study, concentric tube injection with a gaseous fuel is assumed with the drop radius from equation (37) used in equation (35) to calculate the generalized length for the oxidizer. For the gaseous fuel case,  $\mathcal{G}$  is equal to 1.0 with the efficiency due to incomplete vaporization of the oxidizer computed from

$$\bar{\eta}_{\text{vap}} = \frac{\mathcal{G} \left[ \mathcal{O} \left( \frac{\bar{O}}{\bar{F}} \right) \right] \frac{\bar{w}_o}{\bar{w}_o + \bar{w}_f}}{\mathcal{G} \left[ \left( \frac{\bar{O}}{\bar{F}} \right) \right] \frac{\bar{w}_o}{\bar{w}_o + \bar{w}_f}} \quad (\text{gaseous fuel}) \quad (38)$$

where  $\mathcal{G}$  denotes the functional relation of  $c_{\text{th}}^*$  to mixture ratio.

Since the introduction of a swirl to the injected oxidizer stream will tend to enhance the atomization of the oxidizer, equation (37) was multiplied by 0.448. This factor was based on available unpublished data for injectors having swirl elements.

A suitable mixing model for calculation of  $\bar{\eta}_{\text{mix}}$  was not available. Experimental data would be required to allow the use of a mixing model such as the one proposed in reference 11. For this study, equations (38) and (31) were used to calculate a value of  $\bar{\eta}_{\text{mix}}$  from an assumed  $\bar{\eta}_{c^*}$  and a calculated  $\bar{\eta}_{\text{vap}}$  at full thrust conditions. This value was assumed to be constant over the entire range of studies performed.

Combustion delay times. - The chamber gas residence time was computed from specified chamber and nozzle geometry and combustion properties as follows:

$$\theta_g = \frac{\bar{\eta}_{c^*} \bar{c}_{\text{th}}^*}{A_t g_c} \left( \frac{\bar{V}}{R_g T} \right)_c \quad (39)$$

Many analyses of chugging (refs. 12 and 13) have shown that the most important factors in determining low-frequency stability are the time delays associated with the atomi-

zation, vaporization, and burning of the propellants. Experiments described in reference 13 were aimed at defining the static relation between dead time and variables such as chamber pressure, mixture ratio, and injection velocity. The work described in references 14 and 15 was based on a dynamic sensitivity of combustion delay to chamber pressure and injection velocity, respectively. This study will consider only a static sensitivity of combustion delay times to the operating conditions.

Studies reported in reference 16 equated the vaporization delay time  $\sigma_v$  to the time required to vaporize 50 percent of the mass of an injected droplet. Time histories of injected droplets (presented in ref. 8) indicate that the average droplet velocity over this length is approximately equal to the injection velocity. Using this information enables one to calculate the vaporization time delay from:

$$\bar{\sigma}_v = \frac{\bar{l}_{50}}{\bar{v}_{ip}} \quad (40)$$

where  $\bar{v}_{ip}$  is the injection velocity of the propellant droplet.

The length required to vaporize 50 percent  $\bar{l}_{50}$  is calculated by solving equation (34) for the chamber length  $l_c$  with the generalized length parameter equal to 0.0699 meter (ref. 8). This value corresponds to a fraction vaporized  $\phi$  of 0.5 and applies for all propellants. The nozzle term in equation (34) is neglected for this calculation. The resulting expression for  $l_{50}$  is

$$\bar{l}_{50} = 0.0699 \frac{\epsilon_c^{0.44} \left(1 - \frac{\bar{T}}{T_{cr}}\right)^{0.4} \left(\frac{\bar{r}}{7.62 \times 10^{-5}}\right)^{1.45} \left(\frac{\bar{v}}{30.5}\right)^{0.75} \left(\frac{\mathcal{M}}{100}\right)^{0.35} \left(\frac{H}{3.26 \times 10^5}\right)^{0.8}}{\left(\frac{\bar{P}_c}{2.07 \times 10^6}\right)^{0.66}} \quad (41)$$

For the case studied, the vaporization time delay was computed for the liquid oxidizer only. The gaseous fuel vaporization time  $\bar{\sigma}_{vf}$  was set equal to zero, since the fuel is assumed to be completely vaporized before injection.

The gas-phase mixing and reaction delay  $\bar{\sigma}_m$  was related to the distance from the burning zone  $\bar{l}_{50}$  to the nozzle throat and the gas velocity at the nozzle inlet. Based on stability data from references 2, 3, 5, and 7, the curve shown in figure 3 was generated for

$$\bar{\sigma}_m = \mathcal{G} \left[ \frac{10^3 (l_c + l_n - \bar{l}_{50})}{\bar{v}_c} \right] \text{sec} \quad (42)$$

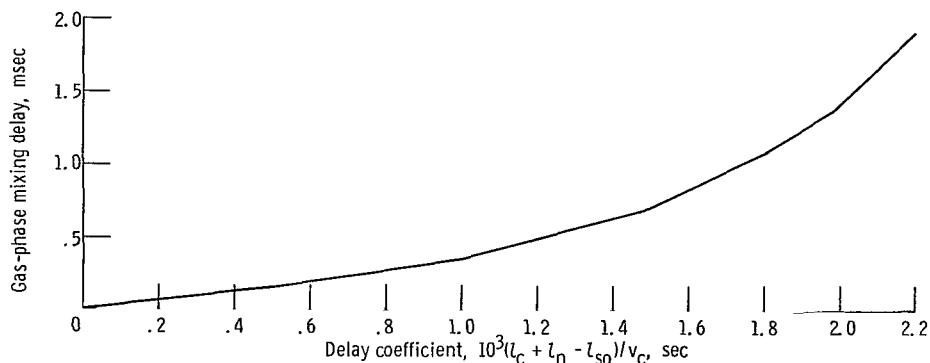


Figure 3. - Gas-phase mixing delay based on experimentally observed chugging frequencies.

where the gas velocity  $\bar{v}_c$  was computed from

$$\bar{v}_c = \bar{M}_c \sqrt{g_c (\gamma R_g \bar{T})_c} \quad \text{m/sec} \quad (43)$$

and  $\mathcal{G}$  represents the functional relation.

Feed system impedances. - Solution of equations (28) and (29) requires evaluation of the imaginary parts of the feed system impedances as functions of frequency. In addition, the critical values of  $\mathcal{R}'_0$  and  $\mathcal{R}'_f$  must be compared with the operating point values to determine stability. Therefore, the computer program must, for a specified feed system configuration, compute the real and imaginary parts of the feed system impedances at the specified frequency  $\omega'$ . This calculation, in general, will involve (1) the breaking up of the feed system into elements, each having a flow impedance  $Z_i$  with real and imaginary parts  $\alpha_i$  and  $\beta_i$ , respectively, (2) the manipulation of these elements (if necessary) into series and parallel combinations, and (3) the stepwise reduction of these combinations using conventional reduction techniques (ref. 17) to obtain the real and imaginary parts of the feed-system impedance.

The resulting values for the series combination of impedances  $Z_i$  and  $Z_j$  (i. e.,  $Z_k = Z_i + Z_j$ ) are

$$\alpha_k = \alpha_i + \alpha_j \quad (44)$$

$$\beta_k = \beta_i + \beta_j \quad (45)$$

For the parallel combination of  $Z_i$  and  $Z_j$  [ $Z_k = Z_i Z_j / (Z_i + Z_j)$ ] the real and imaginary parts of  $Z_k$  are

$$\alpha_k = \frac{\alpha_j (\alpha_i^2 + \beta_i^2) + \alpha_i (\alpha_j^2 + \beta_j^2)}{(\alpha_i + \alpha_j)^2 + (\beta_i + \beta_j)^2} \quad (46)$$

$$\beta_k = \frac{\beta_j (\alpha_i^2 + \beta_i^2) + \beta_i (\alpha_j^2 + \beta_j^2)}{(\alpha_i + \alpha_j)^2 + (\beta_i + \beta_j)^2} \quad (47)$$

Equations (44) to (47) form the basis for calculating the feed-system impedances at the frequency of interest regardless of the feed-system configuration.

Using a lumped-parameter approach allows the liquid feed systems to be divided into the following elements:

(1) Lossless lines having only momentum pressure drop. The flow impedance consists of  $\alpha = 0$  and  $\beta = \omega l / Ag_c$ , where  $l$  is the line length and  $A$  is the cross-sectional area of the line. The electrical analog of this element is an inductance.

(2) Orifices and valves having no momentum pressure drop and flow impedance consisting of  $\alpha = 2 \Delta P / \bar{w}$  and  $\beta = 0$ , where  $\Delta P$  and  $\bar{w}$  are the steady-state pressure drops across the element and flow, respectively. The electrical analog of this element is a resistance.

(3) Storage volumes having a shunt impedance consisting of  $\alpha = 0$  and  $\beta = -Bg_c / \omega \rho V_g$ , where  $B$  is the liquid bulk modulus and  $V$  is the storage volume. The electrical analog of this element is a shunt capacitance.

(4) A pump having no momentum pressure drop or storage. The pump is described by a normalized pressure-rise characteristic; that is,

$$\left. \begin{aligned} \psi_p &= \mathcal{G}(\varphi_p) \\ \Delta P_p &= K_{1p} \psi_p N_p^2 \\ \varphi_p &= \frac{K_{2p} \dot{w}_p}{N_p} \end{aligned} \right\} \quad (48)$$

For the frequencies of interest, the pump speed is assumed to be invariant with time, and the pump impedance consists of  $\alpha = -K_{1p} K_{2p} \bar{N}_p (d\psi_p / d\varphi_p)$  and  $\beta = 0$ , where

$\bar{N}_p$  is the steady-state pump speed and  $d\psi_p/d\phi_p$  is the slope of the pump characteristic at the operating point. The negative sign in the equation for  $\alpha$  arises from the fact that the  $\Delta P$  in equation (48) is a pressure rise, and the impedance  $d\Delta P/d\dot{w}$  is defined in terms of a pressure drop. It should be noted that operation is usually limited to that portion of the characteristic having a negative slope, giving an electrical analog of a positive resistance.

Figure 4 is a schematic of the expander cycle engine to be studied. In this cycle, the fuel passes through a cooling jacket, which surrounds the combustion chamber. The

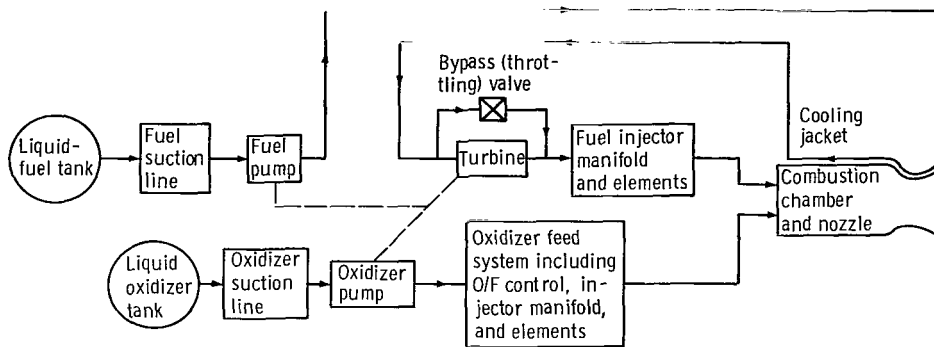


Figure 4. - Schematic of bipropellant engine system using expander cycle.

fuel is vaporized in the jacket and is used to drive a turbine before being injected into the combustion chamber. For the system shown, geared pumps are driven by the turbine supplying high-pressure propellants to the feed system. A turbine-bypass valve is shown; its function is to adjust the engine thrust by varying the amount of fuel passing through the turbine (hence, speed). A control valve is located in the liquid oxidizer system to maintain the desired mixture ratio in the chamber for all thrust levels.

To test the computer program it was decided to study two oxidizer feed systems that would represent two degrees of difficulty in the evaluation of the oxidizer feed system impedance. Figure 5 shows an impedance representation of the two systems considered for this study. Figure 5(a) shows a conventional single-orifice injector supplied by a manifold volume (capacitance). The injector elements consist of several long injection tubes (inductances) with pressure drop (resistance) controlled by orifices immediately upstream of the injection tubes. The tubes are long enough to guarantee steady entrance conditions at the chamber entrance. With a concentric-tube injector, the injector tubes are surrounded by annuli through which the gaseous fuel is injected. The oxidizer manifold is fed by a control valve (resistance) whose area is adjusted to maintain the mixture ratio. A pump discharge volume (capacitance) is located between

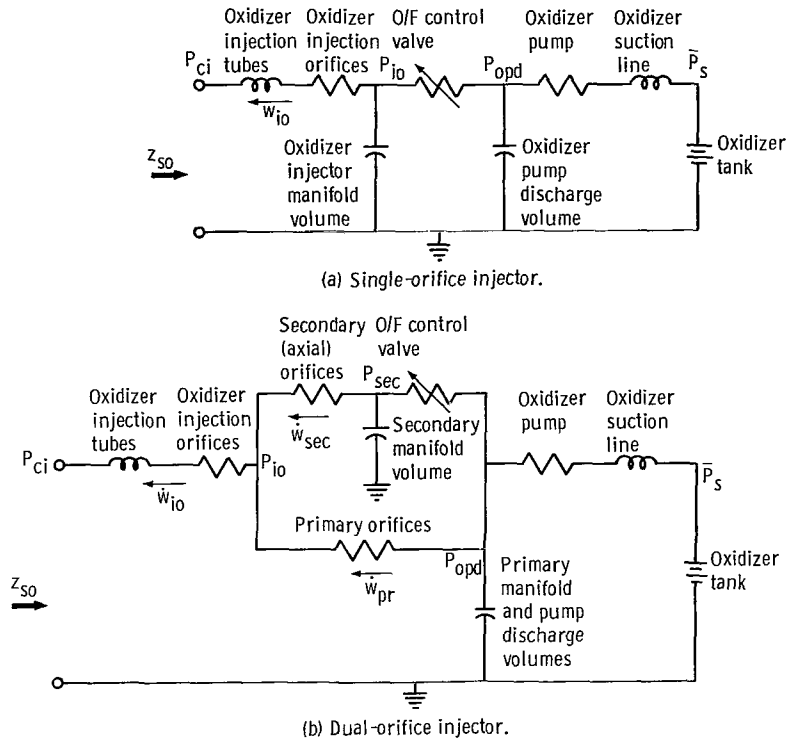


Figure 5. - Impedance representation of two oxidizer feed systems.

the pump (resistance) and the control valve. The pump is assumed to be fed by a tank (battery) and a lossless suction line (inductance).

Figure 5(b) shows a dual-orifice oxidizer injector and feed system. The conventional injection tubes and orifices are fed by two flow components. After discharging from the pump into a pump discharge volume, the flow is split. The bulk of the flow passes through a mixture-ratio control valve and into a secondary-flow manifold (capacitance) which in turn feeds several secondary (axial) orifices. The remaining portion of the flow is collected in a primary manifold (The capacitance is lumped with the pump discharge capacitance.) and distributed to a number of tangential orifices. For this study, each axial orifice had three associated tangential orifices. The tangential flow mixes with the axial flow in an annular chamber imparting a swirl to the injected flow stream. The vortexing action of the tangential flow (ref. 18) maintains the swirl at extremely low thrust (flow) levels enhancing the mixing of the oxidizer stream and the gaseous fuel. For a particular thrust level, the area of the axial orifices is adjusted

statically in the computer program to satisfy the following assumed vortex characteristic:

$$\frac{\bar{w}_{\text{sec}}}{\bar{w}_o} = -2.45 \left( \frac{\bar{P}_{\text{opd}}}{\bar{P}_{\text{sec}}} \right)^2 + 4.52 \frac{\bar{P}_{\text{opd}}}{\bar{P}_{\text{sec}}} - 1.1259 \quad (49)$$

Appendix C outlines the evaluation of the real and imaginary parts of the oxidizer feed systems shown in figure 5. At a particular operating point and frequency, the impedance  $Z_{\text{so}}$  can be expressed as

$$\left. \begin{aligned} Z_{\text{so}}(j\omega') &= \bar{\mathcal{R}}_o + j\bar{\mathcal{I}}_o \\ \bar{\mathcal{R}}_o &= \bar{a} + \bar{\mathcal{A}}(\omega') \\ \bar{\mathcal{I}}_o &= \omega'b + \bar{\mathcal{B}}(\omega') \end{aligned} \right\} \quad (50)$$

where

$\bar{a}$  oxidizer injection orifice resistance  $2 \Delta P / \bar{w}$

$b$  injection tube inductance

The imaginary part  $\bar{\mathcal{I}}_o$  is used in the solution of equations (23) and (24). The real part  $\bar{\mathcal{R}}_o$  will be compared with the critical value  $\mathcal{R}'_o$  resulting from the solution of equation (23). By assuming that the injector geometry allows changes in the orifice resistance  $\bar{a}$  without affecting either the parameters required to solve equation (28) or the rest of the feed system impedance  $\bar{\mathcal{A}}(\omega')$ , the critical value of  $\bar{a}$  can be found from

$$a' = \mathcal{R}'_o - \bar{\mathcal{A}}(\omega') \quad (51)$$

where  $\bar{\mathcal{A}}(\omega')$  is calculated at the selected operating point as outlined in appendix C.

Although the same procedures hold for the evaluation of the fuel impedance  $Z_{\text{sf}}$ , some assumptions are required to conveniently handle the system shown in figure 4. It was physically realistic and mathematically expedient to assume a choked turbine and bypass valve. Assuming steady conditions upstream of the turbine, the fuel injector can be considered to be fed by a constant fuel flow. Since the fuel is vaporized in the cooling jacket, the compressibility of the fuel must be considered in the evaluation of

$Z_{sf}$ . The following equation can be used to compute the fuel flow rate through the injector annuli for isothermal flow with low Mach number:

$$\dot{w}_{if} = K_f \left( \frac{P_{if}^2 - P_{ci}^2}{\bar{T}_f} \right)^{0.5} \quad (52)$$

The steady-state fuel injection velocity  $\bar{v}_f$ , which is required for the calculation of drop size, is computed from

$$\bar{v}_f = (R_g \bar{T})_f \frac{\bar{w}_f}{\bar{P}_{ci}} A_f \quad (53)$$

Linearization and transformation of equation (52) yields

$$\tilde{w}_{if}(S) = \left( \frac{\bar{P}_{if} \bar{w}_f}{\bar{P}_{if}^2 - \bar{P}_{ci}^2} \right) \tilde{P}_{if}(S) - \left( \frac{\bar{P}_{ci} \bar{w}_f}{\bar{P}_{if}^2 - \bar{P}_{ci}^2} \right) \tilde{P}_{ci}(S) \quad (54)$$

For constant fuel flow into the fuel injector manifold, perturbations in the injector manifold pressure can be expressed as

$$\tilde{P}_{if}(S) = - \left( \frac{R_g \bar{T}}{V} \right)_f \frac{\tilde{w}_{if}(S)}{S} \quad (55)$$

where

$\bar{T}_f$  steady-state turbine discharge temperature

$V_f$  fuel injector manifold volume

Combining equations (54) and (55) and letting  $S = j\omega'$  yield

$$\left. \begin{aligned}
Z_{sf}(j\omega') &= \bar{\mathcal{A}}_f + j\bar{\mathcal{J}}_f = \frac{\tilde{P}_{if}(s) - \tilde{P}_{ci}(s)}{\tilde{w}_{if}(s)} \\
\bar{\mathcal{A}}_f &= \frac{\bar{P}_{if}^2 - \bar{P}_{ci}^2}{\bar{P}_{ci}\bar{w}_f} \\
\bar{\mathcal{J}}_f &= -\frac{1}{\omega'} \frac{\bar{P}_{if}}{\bar{P}_{ci}} \left( \frac{R_g \bar{T}}{V} \right)_f
\end{aligned} \right\} \quad (56)$$

The imaginary part  $\bar{\mathcal{J}}_f$  is used in the solution of equations (28) and (29). The real part  $\bar{\mathcal{A}}_f$  can be compared with the critical value  $\mathcal{A}'_f$  resulting from the solution of equation (29), by neglecting the effects of changing  $\mathcal{A}_f$  (change in fuel annulus area) on the imaginary part.

Critical values of the pressure upstream of the injection elements and the corresponding ratios of pressure drop to chamber pressure are found from

$$\bar{P}'_{io} = \frac{a'\bar{w}_o}{2} + \bar{P}_{ci} \quad \left( \frac{\Delta\bar{P}_{io}}{\bar{P}_c} \right)' = \frac{a'\bar{w}_o}{2\bar{P}_c} \quad (57)$$

$$\bar{P}'_{if} = \left( \mathcal{A}'_f \bar{w}_f \bar{P}_{ci} + \bar{P}_{ci}^2 \right)^{1/2} \quad \left( \frac{\Delta\bar{P}_{if}}{\bar{P}_c} \right)' = \frac{\bar{P}'_{if} - \bar{P}_{ci}}{\bar{P}_c} \quad (58)$$

## DIGITAL COMPUTER PROGRAM

A digital computer program, capable of generating stability limits over a wide range of operating conditions and engine configurations, was developed. The stability program was written in FORTRAN IV language for use with the IBM 7094 computer. The program is structured to carry out sequentially the following operations: (1) Calculation, for a specified chamber pressure and from given input data, of the steady-state frequency-insensitive parameters required to solve equations (28) and (29), (2) calculation, for each selected frequency, of the feed system impedances using the procedures outlined in appendix C, (3) for each selected frequency, solution of equations (28) and (29) for the

critical parameters  $\mathcal{R}'_o$  and  $\mathcal{R}'_f$ , (4) translation of the parameters  $\mathcal{R}'_o$  and  $\mathcal{R}'_f$  into pressure drop ratios using equations (57) and (58) (If the results are non-negative, compare with the steady-state operating values to gage the stability margin.) (5) repetition of the preceding steps for each specified chamber pressure or changes in system parameters.

## Steady-State Operating Point

Because of the unavailability of a suitable model for calculating  $\bar{\eta}_{mix}$ , the overall combustion efficiency  $\bar{\eta}_{c*}$  or flow rates at full thrust must be given. Other required input data are (1) chamber, injector, and feed-system geometry, (2) propellant properties, (3) combustion properties for the specified propellant combination, (4) oxidizer pump characteristic, (5) assumed fuel temperature, and (6) O/F control-valve area against chamber pressure for the system shown in figure 4.

The program will calculate the steady-state frequency-insensitive parameters required for the solution of equations (28) and (29) in the following order:

- (1) The propellant properties  $\bar{T}_o$ ,  $\bar{\mathcal{M}}_o$ , and  $\bar{H}_o$  are used to calculate the associated terms in equation (34).
- (2) The specified throat area, characteristic length  $L^* = (V_c + V_n)/A_t$ , contraction ratio, and total length  $l_c + l_n$ , are used to calculate the geometric term in equation (34).
- (3) For a selected chamber pressure  $\bar{P}_c$ , the fuel temperature and O/F control-valve area are calculated using supplied characteristics.
- (4) For the selected chamber pressure and specified mixture ratio,  $\bar{c}_{th}^*$  is computed from input data.
- (5) At full thrust, the overall efficiency  $\eta_{c*}$  is computed from chamber pressure and specified flows. At off-design chamber pressures, an assumed value of  $\eta_{c*}$  (or last computed value) is used to calculate flows.
- (6) From selected chamber pressure and mixture ratio,  $\bar{\gamma}_c$ ,  $\bar{M}_c$ ,  $R_{gc}$ ,  $\bar{T}_c$ , and  $\bar{v}_c$  are computed to allow calculation of chamber pressure at the injector face  $\bar{P}_{ci}$  from equation (23).
- (7) Using input data for the injector, the fuel velocity  $\bar{v}_f$  and fuel injector pressure  $\bar{P}_{if}$  are calculated from equations (52) and (53), and oxidizer velocity and injection orifice pressure drop are calculated assuming a square-law characteristic.
- (8) Using input data for the oxidizer feed system, the steady-state pressure drops across the O/F control valve and dual-orifice elements (if required) are calculated. The program iterates to find the axial-element size which satisfies the vortex characteristic in equation (49) at the specified flow level.

(9) The program computes the oxidizer drop size from equation (37) using the 0.448-swirler-correction factor, the burning length  $\bar{l}_{50}$  from equation (41), the generalized length  $\bar{l}_{gen,o}$  from equation (33), the percent vaporized  $\bar{\theta}$  from the supplied curve from reference 8,  $\bar{\eta}_{vap}$  from equation (32), and the oxidizer vaporization delay  $\bar{\sigma}_{vo}$  from equation (40).

(10) At full thrust,  $\bar{\eta}_{mix}$  is computed from  $\bar{\eta}_{c^*}/\bar{\eta}_{vap}$ . At other chamber pressures a previously determined value of  $\bar{\eta}_{mix}$  is used to compute the overall efficiency,  $\bar{\eta}_{c^*} = \bar{\eta}_{mix}\bar{\eta}_{vap}$ . If the new value does not agree with the assumed value in step (5) the new value is used to recompute flows and repeat steps (7) to (10) until agreement is reached.

(11) Steady-state values of  $\Delta\bar{P}_{io}/\bar{P}_c$  and  $\Delta\bar{P}_{if}/\bar{P}_c$  for comparison with future computed values of the critical ratios as defined in equations (57) and (58).

(12) The gas-residence time,  $\bar{\theta}_g$  from equation (39) and the gas-phase mixing delay  $\bar{\sigma}_m$  from tabular data based on figure 3 are calculated.

(13) The engine gains  $\bar{X}$  and  $\bar{F}$  are computed from equations (14) and (15) with the partial derivative of  $c_{th}^*$  with respect to O/F calculated by the computer at the selected chamber pressure and mixture ratio.

(14) The oxidizer and fuel-system element resistances, inductances, and capacitances are calculated using the appropriate line geometry, manifold volumes, orifice, and valve pressure drops, etc. From the calculated oxidizer pump discharge pressure and specified inlet (tank) pressure, equation (48) can be used to solve for the required steady-state pump speed. This speed value is then used to calculate the pump resistance from the slope of the supplied pump characteristic.

(15) All pertinent information is written out.

## Calculation of Stability Limits

After calculating all of the steady-state frequency-independent parameters required for the solution of equations (28) and (29), a range of possible chugging frequencies to be studied must be specified. Experience has shown that a lower frequency band extending from  $3.5/\tau$  hertz (where  $\tau$  is the sum of the oxidizer-vaporization delay, gas-phase mixing delay, and gas residence time in milliseconds) to about  $4.0/\tau$  hertz and a higher band extending from  $8.7$  to  $12.0/\tau$  hertz will generally enclose the solutions of interest. Depending on the configuration and operating point being studied, solutions in either or both of these bands may exist. For the studies conducted herein, the solutions within a band occurred at frequencies quite close together. For this reason a frequency increment of 0.1 hertz was chosen in both frequency bands.

For the selected steady-state operating point and for each frequency of interest, the following calculations were made by the computer program:

(1) Calculate the steady-state value of the imaginary part of the fuel impedance  $\bar{\mathcal{J}}_f$  using equation (56).

(2) Calculate the real and imaginary parts of the oxidizer impedance  $\bar{\mathcal{A}}_o$  and  $\bar{\mathcal{J}}_o$  using the reduction procedure outlined in appendix C.

(3) Calculate the remaining frequency-dependent parameters which appear in equations (28) and (29).

(4) Solve equation (28) for real solutions of  $\mathcal{A}'_o$  and convert to critical values of injection orifice resistance  $a'$  using equation (51). Disregard negative values of  $a'$

(5) Using results from step (4), calculate the critical value (or values) of  $\mathcal{A}'_f$  using equation (29). Disregard negative values of  $\mathcal{A}'_f$ .

(6) Convert results from steps (4) and (5) into critical values of injection element pressure drop using equation (57) and (58).

(7) Store the results from step (6) together with the frequency and repeat steps (1) to (7) for each frequency in the selected bands of frequency.

(8) Write out the results of steps (1) to (7). An ordering subroutine is included in the program to write out the critical pressure-drop ratios  $(\Delta\bar{P}_{i_o}/\bar{P}_c)'$  and  $(\Delta\bar{P}_{i_f}/\bar{P}_c)'$  and the corresponding frequency in order of increasing  $(\Delta\bar{P}_{i_f}/\bar{P}_c)'$ .

Both the steady-state and stability portions of the program are repeated for each chamber pressure of interest and system parameter value. The existing program is set up to study chamber pressures from 100 to 10 percent of the full thrust value and fuel annulus areas from 25 to 200 percent of the design value.

For both the variable  $\bar{P}_c$  case (throttling) and the variable fuel area case, the only results from the stability portion of the program that are of interest are those sets of points  $((\Delta\bar{P}_{i_f}/\bar{P}_c)')$ ,  $(\Delta\bar{P}_{i_o}/\bar{P}_c)'$ , and  $f' = \omega'/2\pi$  where  $(\Delta\bar{P}_{i_f}/\bar{P}_c)'$  is equal to the steady-state operating value corresponding to the specified fuel annulus area. This is based on the fact that the combustion delay times  $\bar{\sigma}_{v_o}$  and  $\bar{\sigma}_m$  are sensitive to the fuel injection velocity and the stability limits are generated using the steady-state operating value of fuel velocity. For this reason, interpolation of the results written out in step (8) of the stability portion of the program is required. For the variable fuel area case, this interpolation is built into the program. For the throttling case, the interpolation can be handled conveniently by hand from the output data because of the small variation of frequency along the boundary.

Appendix D contains a list of the computer program symbols and their definitions. Appendix E contains a computer listing showing the actual implementation of the steps outlined in the steady-state and stability subprogram discussion. The indexing shown corresponds to the case of a dual-orifice injector configuration (see fig. 5(b)) at full thrust with varying fuel annulus area. Comment cards are inserted at appropriate loca-

tions in the listing to aid in the understanding of the program. Also shown is a printout of the resultant stability limits for this system together with other pertinent information. The computer program as shown in the listing, is set up for the expander cycle with gaseous fuel being fed into the injector manifold at a constant rate. The programming of the general liquid-liquid system, as described in the analysis, requires the calculation of both oxidizer and fuel vaporization delays, gas-phase delays, feed system impedances, etc.

Appendix F contains a flow chart for the digital program and a discussion, which is intended as a guide for users of the program. This information, together with the comment cards contained in the listing (appendix E), should help the user to modify the program to study different engine configurations. The steps required to analyze liquid-liquid propellant systems are also discussed in appendix F.

## RESULTS AND DISCUSSION

### Single-Orifice Configuration

A flox-methane engine system using an expander cycle and an oxidizer injector as shown in figure 5(a) was studied using the digital program. Table I shows the specified full thrust values of the chamber pressure, flows, etc.

At full thrust ( $\bar{P}_c = 3.45 \times 10^6 \text{ N/m}^2$ ) the steady-state and stability portions of the program were used to determine critical injector pressure drops for a range of fuel injector annulus areas. Figure 6 is a plot of the digital data. For the nominal fuel area, the ratio of fuel-injector-pressure drop to chamber pressure ( $\Delta\bar{P}_{if}/\bar{P}_c$ ) is 0.152 at full thrust with a nominal oxidizer ratio of 0.250. For the nominal fuel area, the stability

TABLE I. - SINGLE-ORIFICE CONFIGURATION OPERATING CONDITIONS AT FULL THRUST

Chamber pressure, $P_c$ , $\text{N/m}^2$ . . . . .	$3.45 \times 10^6$
Mixture ratio, O/F . . . . .	5.25
Oxidizer mass flow rate, $\dot{w}_o$ , kg/sec . . . . .	4.68
Fuel mass flow rate, $\dot{w}_f$ , kg/sec . . . . .	0.891
Fuel-injector total pressure, $P_{if}$ , $\text{N/m}^2$ . . . . .	$4.02 \times 10^6$
Fuel-injector temperature, $T_{if}$ , K . . . . .	763
Oxidizer-injector total pressure, $P_{io}$ , $\text{N/m}^2$ . . . . .	$4.35 \times 10^6$
Oxidizer pump discharge pressure, $P_{opd}$ , $\text{N/m}^2$ . . . . .	$4.69 \times 10^6$
Oxidizer tank pressure, $P_{To}$ , $\text{N/m}^2$ . . . . .	$2.76 \times 10^5$
Oxidizer pump speed, $N_o$ , rpm . . . . .	$2.465 \times 10^4$
Oxidizer velocity, $v_o$ , m/sec . . . . .	20.42
Fuel velocity, $v_f$ , m/sec . . . . .	214.4

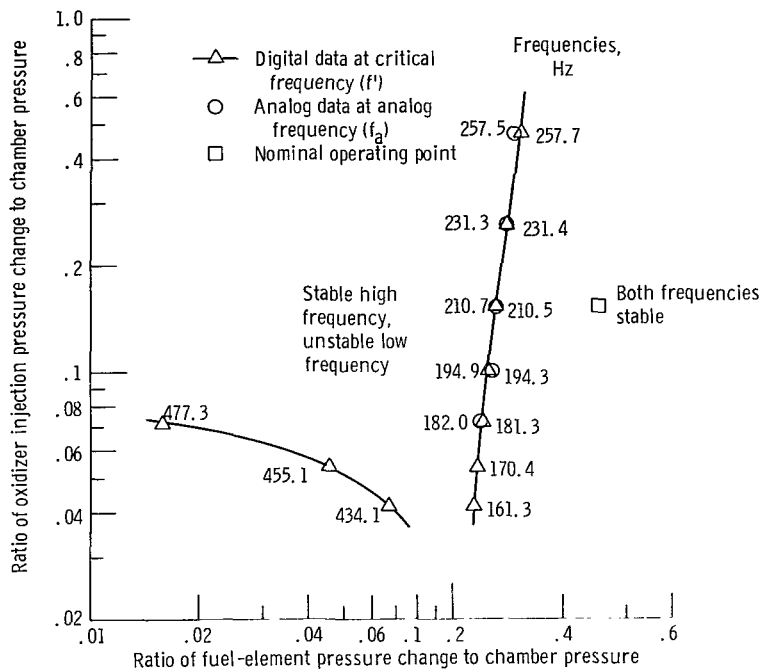


Figure 6. - Comparison of analog and digital stability limits for single-orifice, full-thrust injector with varying fuel area. Delays sensitive to fuel area.

program yielded a critical oxidizer ratio of 0.130, which indicates stable operation with the nominal geometry. At the critical oxidizer ratio, a chugging frequency of 210.5 hertz was determined by the program. Changes in the oxidizer pressure drop are assumed to be made by changing the size of the oxidizer injection orifice without affecting the injection velocities, delay times, etc. If one assumes that the resulting changes in pressures, upstream of the injector, have only second-order effects on the stability of the engine, then the difference between the operating point and critical pressure drops represents the stability margin at the operating point. A stability boundary was formed by computing critical oxidizer pressure drops for various fuel annulus areas. For each selected fuel area, the delay times were calculated using the steady-state operating point portion of the program. Figure 6 also shows a higher frequency boundary at lower oxidizer and fuel pressure-drop ratios. For these operating conditions, the higher frequency boundary is not important since the lower frequency boundary will determine the stability of operation. For comparison with digital results, results from an analog computer simulation are also shown. On the analog computer, a small-impulse disturbance was introduced in the rate of change of burned products ( $\Delta \dot{w}_p$  as shown in fig. 2) with a resulting sinusoidal oscillation in chamber pressure. The oxidizer injection orifice size was slowly decreased while adjusting the pump speed to maintain flow until steady-amplitude oscillations in chamber pressure were observed. Frequencies on the analog

were determined by using an electronic counter which gave a visual indication of the oscillation period (in msec). Excellent agreement in the boundary location and frequency is indicated in figure 6, which substantiates the inference of stability margin from the digital data. In terms of stability, a slight advantage in decreasing the fuel-injector pressure drop is indicated. A study of the computer results, however, indicated a loss in combustion efficiency due to a decrease in the injection momentum ratio. This results in an increase in drop-size, and in decreases in the generalized length parameter  $l_{gen}$  and fraction vaporized  $\phi$  for the oxidizer. Although the combustion efficiency due to mixing is assumed constant ( $\eta_{mix} = 0.973$ ), the decrease in momentum ratio would probably result in a further decrease in performance due to incomplete mixing.

The effect of throttling the engine at constant mixture ratio was also studied. A turbine-bypass valve (see fig. 4) was assumed to control chamber pressure through pump speed. A mixture ratio control valve (fig. 5(a)) area was varied in a specified manner to maintain the chamber mixture ratio. Using the nominal fuel area, the steady-state and stability portions of the program were run for various chamber pressures. Figure 7 shows the results from the digital program. Figure 7(a) shows a plot of the critical values  $(\Delta \bar{P}_{if}/\bar{P}_c)'$  and  $(\Delta \bar{P}_{io}/\bar{P}_c)'$  at full thrust together with the frequency  $f' = \omega'/2\pi$ . Since all points on the boundary were computed using the operating point delay times, the only boundary point of interest corresponds to the operating value of fuel-injector pressure drop.

Interpolation on the plot yields the critical value of oxidizer pressure-drop ratio equal to 0.130 and frequency about 210 hertz which agrees with the results shown in figure 6. As chamber pressure was decreased (figs. 7(b) and (c)) a shift in the lower frequency boundary to the left is observed with the operating point moving upward and to the left. The upward movement of the operating point is due to the assumed static relation between turbine discharge temperature and chamber pressure. At a throttling ratio of 3.33, figure 7(d) shows the appearance of a higher frequency boundary from the left. No lower frequency boundary is indicated since at this operating point, the valve and pump impedances are sufficient to stabilize the lower frequency mode. Figure 7(e) shows that at a throttling ratio of 5, a higher frequency instability is predicted at a frequency of 529 hertz. Figure 7(f) is a plot of the critical oxidizer pressure drop ratios at the operating point value of fuel pressure drop against the throttling ratio. By neglecting the second-order effects on stability of changing the pressure level upstream of the injector, the difference between the throttling path and the boundaries can be considered to be the stability margin of the engine. For throttling ratios between 2.0 and 2.5, no injection orifice pressure drop is required. The limiting factor on throttling appears to be the higher frequency instability with a throttling limit of 4.82.

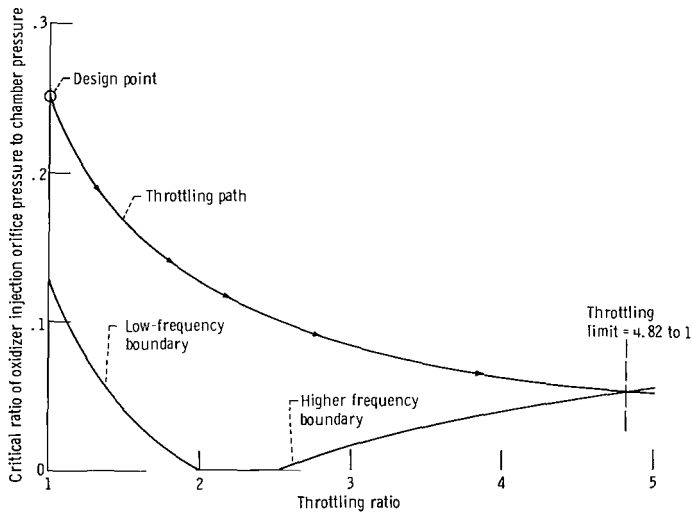
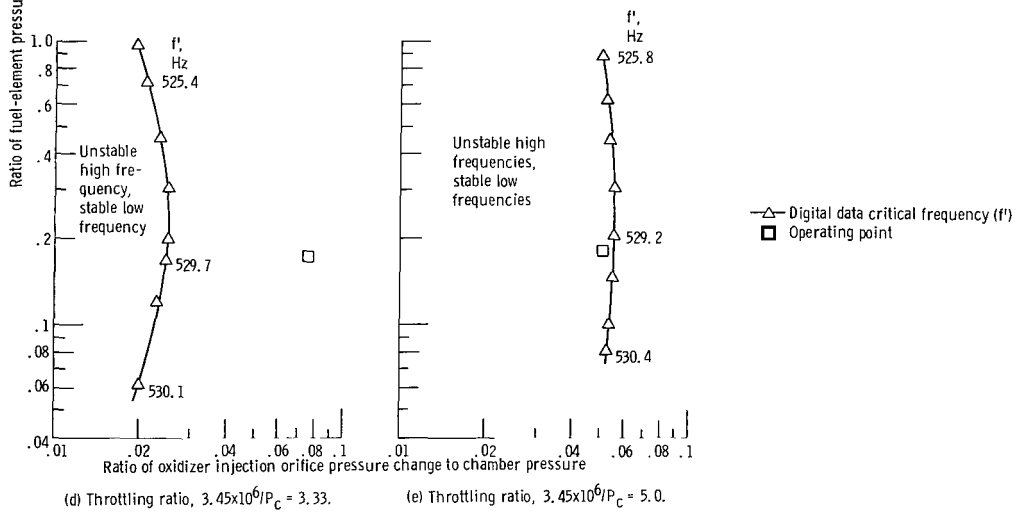
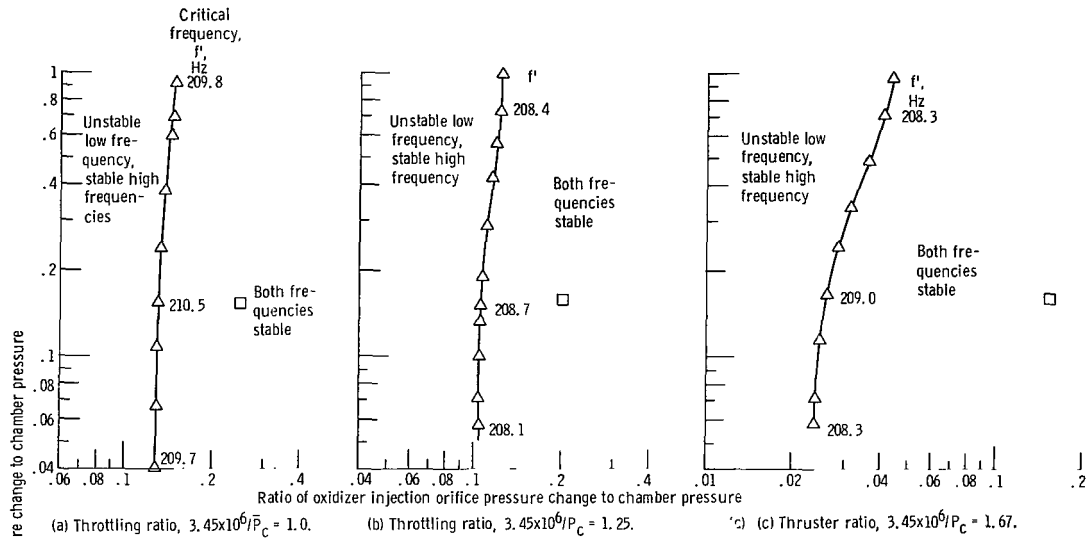


Figure 7. - Digital results for stability limits for single-orifice, nominal-fuel area injector. Delays evaluated at operating point.

## Dual-Orifice Configuration

A flox-methane engine system using an expander cycle and an oxidizer injector as shown in figure 5(b) was studied using the digital program. Table II shows the specified full thrust operating conditions for this configuration. Figure 8 shows the plot of digital data showing the effect of varying fuel annulus area and oxidizer injection orifice size on the stability limits at full thrust. For this configuration more advantage is indicated for decreasing the fuel injector pressure drop ratio. Digital data indicated that operation at a fuel injector pressure drop ratio of 0.15 (same as single-orifice case) could be accomplished with no performance degradation due to incomplete vaporization. Appendix E contains a printout of the digital results for this case. Figure 8 also shows the higher frequency boundary dominating the stability at fuel-injector pressure drops below about  $0.1 \bar{P}_c$ . Analog computer results are also shown in figure 8. Excellent agreement between analog and digital data were obtained. Unfortunately, a limitation of the analog time delay capability prevented any determination of the higher frequency boundary on the analog. Analog computer operation in the stable-low, unstable-high frequency region has been achieved for other engine configurations. Figure 9 shows the response of chamber pressure to an impulse disturbance in flow for oxidizer injector pressure-drop ratios both greater than and less than the critical value. Figure 9(a) shows the decay of oscillations for stable operation with both frequencies apparent in the trace. Figure 9(b) shows a decay in the low-frequency component but a growing higher frequency component.

The effect of throttling the dual orifice system at constant mixture ratio was also studied using the digital program. As in the case of the single orifice injector a turbine bypass throttle was assumed with mixture-ratio controlled by a valve in the secondary

TABLE II. - DUAL ORIFICE CONFIGURATION OPERATING CONDITIONS AT FULL THRUST

Chamber pressure, $P_c$ , $N/m^2$ . . . . .	$3.46 \times 10^6$
Mixture ratio, O/F . . . . .	5.25
Oxidizer mass flow rate, $\dot{w}_o$ , kg/sec . . . . .	4.74
Fuel mass flow rate, $\dot{w}_f$ , kg/sec . . . . .	0.903
Primary flow mass flow rate, $\dot{w}_{pr}$ , kg/sec . . . . .	0.479
Secondary flow mass flow rate, $\dot{w}_{sec}$ , kg/sec . . . . .	4.27
Secondary total pressure, $P_{sec}$ , $N/m^2$ . . . . .	4.03
Oxidizer injector total pressure, $P_{io}$ , $N/m^2$ . . . . .	$3.84 \times 10^6$
Fuel injector total pressure, $P_{if}$ , $N/m^2$ . . . . .	$4.52 \times 10^6$
Fuel injector temperature, $T_{if}$ , K . . . . .	747
Oxidizer pump discharge pressure, $P_{opd}$ , $N/m^2$ . . . . .	$4.35 \times 10^6$
Oxidizer tank pressure, $P_{To}$ , $N/m^2$ . . . . .	$2.76 \times 10^5$
Oxidizer pump speed, $N_o$ , rpm . . . . .	$2.396 \times 10^4$
Oxidizer velocity, $v_o$ , m/sec . . . . .	12.92
Fuel velocity, $v_f$ , m/sec . . . . .	217.1

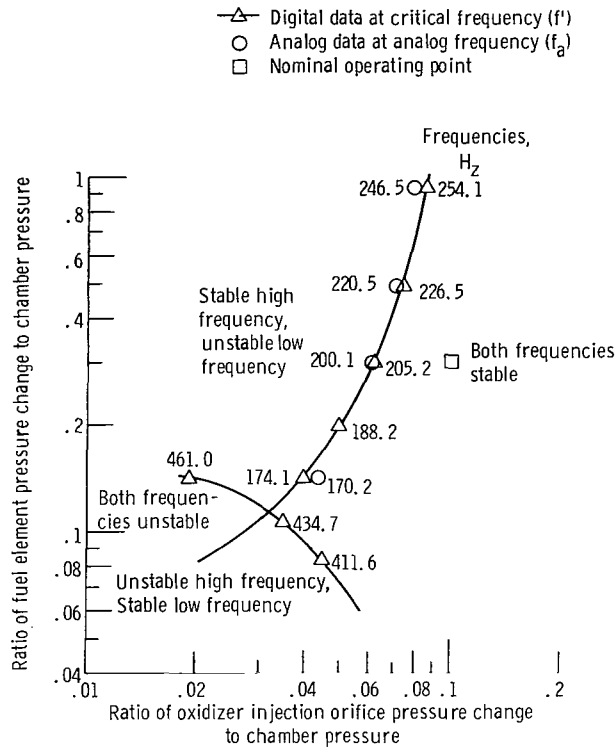
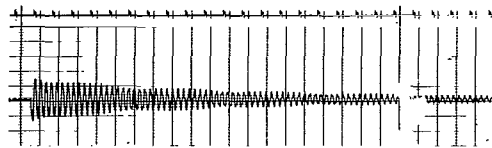
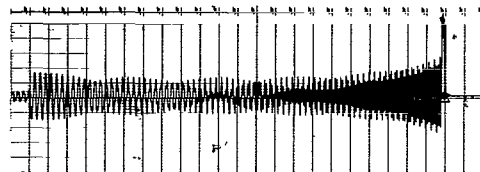


Figure 8. - Comparison of analog and digital stability limits for dual-orifice, full-thrust injector with varying fuel area. Delays sensitive to fuel area.



(a) Oxidizer injection orifice pressure change greater than critical.



(b) Oxidizer injection orifice pressure change less than critical.

Figure 9. - Response of chamber pressure to pulse-type disturbance on analog for conditions where higher frequency is unstable and lower frequency is stable.

(axial) flow path (see fig. 5(b)). Figure 10 shows the results of the throttling study. Figures 10(a) and (b) show stable operation for throttling ratios of 1 to 1.43. At a throttling ratio of 3.33, the higher frequency boundary appears from the left in figure 10(c) with frequencies around 502 hertz at the boundary. Figure 10(d) shows near neutrally stable operation at a throttling ratio of 5.0 with a chugging frequency of 493 hertz. Figure 10(e) shows the movement of the operating point and stability margin for varying thrust. Figure 10(e) indicates a throttling limit of 4.8 which agrees with the single-orifice result.

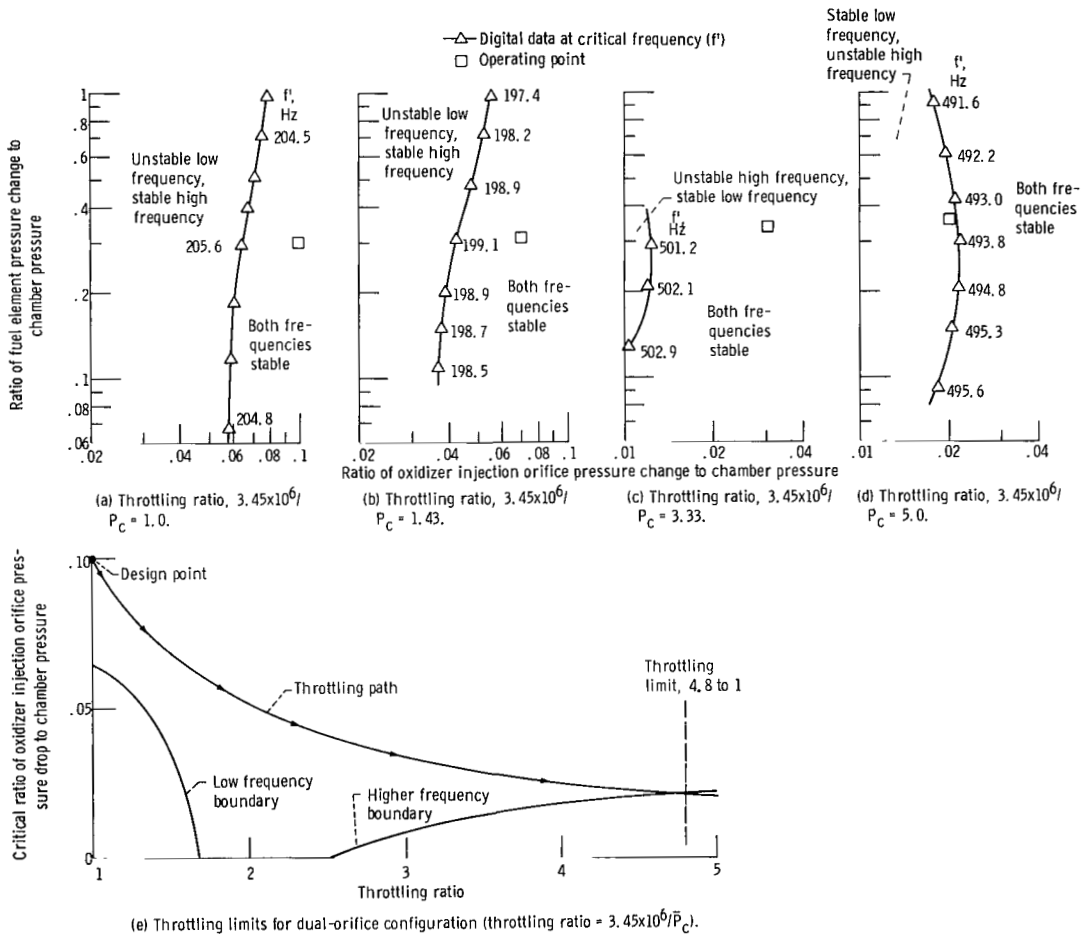


Figure 10. - Digital results for stability limits for dual-orifice, nominal-fuel area injector. Delays evaluated at operating point.

## CONCLUDING REMARKS

A digital program has been developed to determine stability limits for throttleable, bipropellant rocket engines. The program was written in FORTRAN IV language for use with the IBM 7094 computer.

The program consists of (1) a steady-state operating point subprogram which computes required parameters for solution of the characteristic equation and (2) a stability subprogram which solves the characteristic equation for critical values of the injection element pressure drops over a range of chugging frequency. Guidelines are provided for choosing the range of frequency to be studied.

Available vaporization and drop size correlations are used to compute vaporization efficiencies and combustion delay times. The effects of injector geometry, valve resistance, pump characteristics, suction line inductance, etc., are included in the basic program.

Digital stability data were computed for an expander cycle engine using (1) a conventional single-orifice concentric-tube injector and (2) a dual-orifice concentric-tube injector. The effects of throttling at constant mixture ratio and of varying the injector pressure drops at full thrust on stability were determined. Excellent agreement between digital and analog computer data were obtained.

For both injector configurations, throttling was limited to about 5 because of higher frequency instabilities (about 500 Hz), which is characteristic of the double-dead-time model used in the program. For the dual-orifice configuration, results indicated that the design-point fuel-injector pressure drop could be decreased by 50 percent without degrading performance or stability.

The development and workings of the computer program were discussed in detail and a program listing, together with a typical printout of results are provided.

Lewis Research Center,  
National Aeronautics and Space Administration,  
Cleveland, Ohio, September 8, 1970,  
128-31.

## APPENDIX A

### SYMBOLS

<p>A cross-sectional area, <math>m^2</math></p> <p><math>\mathcal{R}</math> real part of oxidizer feed system impedance, excluding injection orifice resistance, <math>((N)(sec)/(m^2)(kg))</math></p> <p><math>A_t</math> throat area, <math>m^2</math></p> <p>a oxidizer injection orifice resistance, <math>((N)(sec)/(m^2)(kg))</math></p> <p>B bulk modulus of liquid, <math>N/m^2</math></p> <p><math>\mathcal{I}</math> imaginary part of oxidizer feed system impedance, excluding injection tube reactance, <math>((N)(sec)/(m^2)(kg))</math></p> <p>b oxidizer injection tube inductance, <math>((N)(sec^2)/(m^2)(kg))</math></p> <p><math>c^*</math> characteristic velocity, <math>m/sec</math></p> <p>d diameter, <math>m</math></p> <p>F partial derivative of chamber pressure with respect to fuel flow as defined by eq. (15), <math>((N)(sec)/(m^2)(kg))</math></p> <p><math>\mathcal{F}</math> fraction of fuel vaporized</p> <p>f frequency, <math>Hz</math></p> <p><math>\mathcal{G}</math> denotes functional relation</p> <p>g gravitational acceleration, <math>9.8 m/sec^2</math></p> <p><math>g_c</math> gravitational constant, <math>1 (kg)(m)/(N)(sec^2)</math></p> <p>H heat of vaporization for liquid, <math>J/kg</math></p>	<p><math>\mathcal{I}</math> imaginary part of feed system impedance, <math>((N)(sec)/(m^2)(kg))</math></p> <p><math>K_c</math> chamber momentum loss coefficient as defined by eq. (23)</p> <p><math>K_f</math> fuel-injector flow coefficient as defined by eq. (52), <math>((kg)(m^2)(K^{1/2})/(sec)(N))</math></p> <p><math>K_r</math> drop size coefficient as defined by eq. (35)</p> <p><math>K_{1p}</math> pump pressure rise coefficient as defined by eq. (48), <math>((N)(sec^2)/(m^2))</math></p> <p><math>K_{2p}</math> pump flow coefficient as defined by eq. (48), <math>kg^{-1}</math></p> <p><math>L^*</math> characteristic length, <math>m</math></p> <p><math>l</math> length, <math>m</math></p> <p><math>\mathcal{M}</math> molecular weight for liquid, <math>((kg)/(kg)(mole))</math></p> <p>M Mach number</p> <p>N pump speed, <math>sec^{-1}</math></p> <p><math>\mathcal{O}</math> fraction of oxidizer vaporized</p> <p>O/F mixture ratio</p> <p>P total pressure, <math>N/m^2</math></p> <p>p static pressure, <math>N/m^2</math></p> <p><math>R_g</math> gas constant, <math>J/(kg)(K)</math></p> <p>r drop radius, <math>m</math></p> <p><math>\mathcal{R}</math> real part of feed system impedance, <math>((N)(sec)/(m^2)(kg))</math></p> <p>S Laplace operator, <math>sec^{-1}</math></p>
--	---

$\mathcal{S}$	nozzle shape factor = $V_n/A_c l_n$	$\rho$	mass density, $\text{kg}/\text{m}^3$
T	temperature, K	$\sigma$	time delay, sec
t	time, sec	$\tau$	sum of oxidizer delays and gas residence time, sec
V	volume, $\text{m}^3$	$\varphi$	flow parameter as defined by eq. (43)
v	velocity, $\text{m}/\text{sec}$	$\psi$	pressure-rise parameter as defined by eq. (43)
W	mass, kg	$\omega$	angular frequency, $\text{rad}/\text{sec}$
$\dot{w}$	mass flow rate, $\text{kg}/\text{sec}$	Subscripts:	
X	partial derivative of chamber pressure with respect to oxidizer flow as defined by eq. (14), $((N)(\text{sec})/(\text{m}^2)(\text{kg}))$	a	analog value
Y	substitution parameter as defined in eq. (5)	b	burned
Z	complex flow impedance, $((N)(\text{sec})/(\text{m}^2)(\text{kg}))$	c	chamber (at nozzle inlet)
$\alpha$	real part of general system element impedance, $((N)(\text{sec})/(\text{m}^2)(\text{kg}))$	ci	chamber (at injector face)
$\beta$	imaginary part of general system element impedance, $((N)(\text{sec})/(\text{m}^2)(\text{kg}))$	cr	critical
$\gamma$	specific heat ratio	c*	characteristic velocity
$\Delta P$	total pressure loss (rise for pump), $\text{N}/\text{m}^2$	f	fuel
$\Delta \dot{w}$	disturbance in mass flow rate, $\text{kg}/\text{sec}$	fb	burned fuel
$\delta$	surface tension of liquid, $\text{N}/\text{m}$	gen	generalized
$\epsilon_c$	contraction ratio	i, j, k	indices for general feed system elements
$\eta$	efficiency	if	fuel injector
$\theta_g$	gas residence time as defined by eq. (34), sec	io	oxidizer injector
$\lambda$	real part of complex variable S, $\text{rad}/\text{sec}$	ip	injected propellant droplet
$\mu$	viscosity of liquid, $((N)(\text{sec})/(\text{m}^2))$	m	gas-phase mixing and reaction
		man	manifold
		mix	due to incomplete mixing
		n	nozzle
		o	oxidizer
		$\text{O}_2$	liquid oxygen
		ob	burned oxidizer

opd oxidizer pump discharge  
p pump  
pr primary flow  
s suction line  
sec secondary flow  
sf fuel system output  
so oxidizer system output  
T total  
th theoretical  
V valve

v vaporized  
vap due to incomplete vaporization  
vf vaporized fuel  
vo vaporized oxidizer  
50 50-percent vaporized

Superscripts:

— mean or steady-state value of any variable  
' critical value of any variable  
~ time-varying portion of any variable (i. e.,  $x = \bar{x} + \tilde{x}$ )

## APPENDIX B

### SOLUTION OF CHARACTERISTIC EQUATION

The characteristic equation describing the bipropellant engine system was derived in the text and was

$$-1 = \left[ \frac{\overline{XK}_c}{Z_{so}(S)} e^{-(\bar{\sigma}_{vo} + \bar{\sigma}_m)S} + \frac{\overline{FK}_c}{Z_{sf}(S)} e^{-(\bar{\sigma}_{vf} + \bar{\sigma}_m)S} \right] \frac{1}{\bar{\theta}_g S + 1} \quad (B1)$$

By letting  $S = j\omega'$ ,  $\sigma_{T0} = \sigma_{vo} + \sigma_m$ ,  $\sigma_{Tf} = \sigma_{vf} + \sigma_m$ ,  $Z_{so} = \mathcal{R}'_o + j\mathcal{I}'_o$ , and  $Z_{sf} = \mathcal{R}'_f + j\mathcal{I}'_f$ , the characteristic equation becomes

$$-1 - j\omega\theta_g = \left[ \frac{\overline{XK}_c \cos(\omega\bar{\sigma}_{T0}) - j\overline{XK}_c \sin(\omega\bar{\sigma}_{T0})}{\mathcal{R}'_o + j\mathcal{I}'_o} + \frac{\overline{FK}_c \cos(\omega\sigma_{Tf}) - j\overline{FK}_c \sin(\omega\sigma_{Tf})}{\mathcal{R}'_f + j\mathcal{I}'_f} \right] \quad (B2)$$

By multiplying both sides of equation (B2) by the terms  $(\mathcal{R}'_o + j\mathcal{I}'_o)$  and  $(\mathcal{R}'_f + j\mathcal{I}'_f)$ , separating both sides into real and imaginary parts, and equating reals and imaginaries, the real part of the fuel impedance,  $\mathcal{R}'_f$ , can be solved for using the real and imaginary equations. From the imaginary equation,

$$\frac{1}{\mathcal{R}'_f} = \frac{\mathcal{R}'_o \omega' \bar{\theta}_g + \mathcal{I}'_o - \overline{XK}_c \sin(\omega' \bar{\sigma}_{T0})}{\overline{FK}_c \mathcal{R}'_o \sin(\omega' \sigma_{Tf}) - \overline{FK}_c \mathcal{I}'_o \cos(\omega' \sigma_{Tf}) - \overline{XK}_c \mathcal{I}'_f \cos(\omega' \sigma_{T0}) + \omega' \theta_g \mathcal{I}'_o \mathcal{I}'_f - \mathcal{I}'_f \mathcal{R}'_o} \quad (B3)$$

From the real equation,

$$\frac{1}{\mathcal{R}'_f} = \frac{\omega' \theta_g \mathcal{I}'_o - \mathcal{R}'_o - \overline{XK}_c \cos(\omega' \bar{\sigma}_{T0})}{\overline{FK}_c \mathcal{R}'_o \cos(\omega' \sigma_{Tf}) + \overline{FK}_c \mathcal{I}'_o \sin(\omega' \sigma_{Tf}) + \overline{XK}_c \mathcal{I}'_f \sin(\omega' \sigma_{T0}) - \mathcal{I}'_o \mathcal{I}'_f - \omega' \theta_g \mathcal{I}'_f \mathcal{R}'_o} \quad (B4)$$

Equations (B3) and (B4) yield the following quadratic equation in terms of  $\mathcal{A}'_0$ :

$$\begin{aligned}
 \mathcal{A}'_0{}^2 \left[ Y - \frac{\overline{\mathcal{J}}_f}{\overline{\mathcal{F}}\overline{\mathcal{K}}_c} (1 + \omega'^2 \overline{\theta}_g^2) \right] + \mathcal{A}'_0 \left\{ -\overline{\mathcal{X}}\overline{\mathcal{K}}_c \sin(\omega'\overline{\sigma}_{T_o} - \omega'\overline{\sigma}_{T_f}) - \frac{2\overline{\mathcal{X}}\overline{\mathcal{J}}_f}{\overline{\mathcal{F}}} [\cos(\omega'\overline{\sigma}_{T_o}) - \omega'\overline{\theta}_g \sin(\omega'\overline{\sigma}_{T_o})] \right\} \\
 + \left\{ \overline{\mathcal{J}}_o{}^2 Y - \overline{\mathcal{J}}_o \overline{\mathcal{X}}\overline{\mathcal{K}}_c \cos(\omega'\overline{\sigma}_{T_o} - \omega'\overline{\sigma}_{T_f}) + \frac{2\overline{\mathcal{X}}\overline{\mathcal{J}}_o \overline{\mathcal{J}}_f}{\overline{\mathcal{F}}} [\sin(\omega'\overline{\sigma}_{T_o}) + \omega'\overline{\theta}_g \cos(\omega'\overline{\sigma}_{T_o})] \right. \\
 \left. - \frac{\overline{\mathcal{J}}_f \overline{\mathcal{J}}_o^2}{\overline{\mathcal{F}}\overline{\mathcal{K}}_c} (1 + \omega'^2 \overline{\theta}_g^2) - \frac{\overline{\mathcal{X}}^2 \overline{\mathcal{J}}_f \overline{\mathcal{K}}_c}{\overline{\mathcal{F}}} \right\} = 0
 \end{aligned} \tag{B5}$$

where

$$Y = \omega'\overline{\theta}_g \cos(\omega'\overline{\sigma}_{T_f}) + \sin(\omega'\overline{\sigma}_{T_f})$$

## APPENDIX C

### EVALUATION OF FEED SYSTEM IMPEDANCES

Solution of the characteristic equation for the bipropellant system, as outlined in appendix B, requires the knowledge of the imaginary parts of the feed system impedances  $\mathcal{J}_o$  and  $\mathcal{J}_f$  at each frequency of interest. The following discussion will outline the steps required to evaluate these parameters for both the single and dual injector configurations. In general, the evaluation will involve (1) the breaking up of the feed system in question into its elements, each having a flow impedance  $Z_i$  with the real and imaginary parts  $\alpha_i$  and  $\beta_i$ , respectively, (2) the manipulation of these elements (if necessary) into series and parallel combinations, and (3) the stepwise reduction of these combinations to obtain the feed-system impedance (both real and imaginary parts) at the frequency of interest.

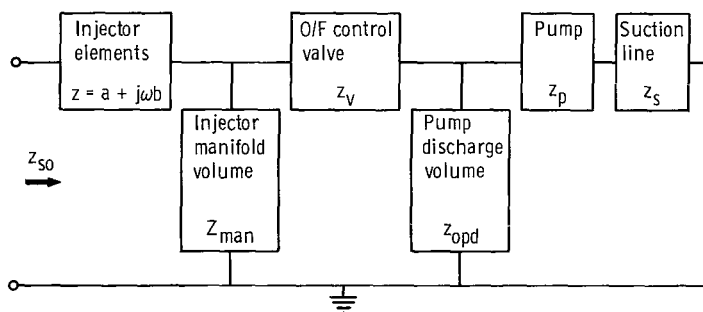


Figure 11. - Impedance representation of single orifice oxidizer feed system.

The step-wise reduction of the system shown in figure 11 would be

$$Z_1 = Z_p + Z_s \quad (C1)$$

$$Z_2 = \frac{Z_1 Z_{opd}}{Z_1 + Z_{opd}} \quad (C2)$$

$$Z_3 = Z_2 + Z_V \quad (C3)$$

$$Z_4 = \frac{Z_3 Z_{\text{man}}}{Z_3 + Z_{\text{man}}} \quad (\text{C4})$$

$$Z_{\text{so}} = Z_4 + a + j\omega b \quad (\text{C5})$$

For this case, the imaginary and real parts of  $Z_{\text{so}}$  would be

$$\mathcal{I}_0 = \omega b + \beta_4 \quad \mathcal{R}_0 = a + \alpha_4 \quad (\text{C6})$$

where  $\beta_4$  is the imaginary part of the impedance  $Z_4$ , evaluated at the frequency of interest. To evaluate the real and imaginary parts of the impedances, the following equations are very useful: If

$$Z_k = Z_i + Z_j$$

then

$$\alpha_k = \alpha_i + \alpha_j$$

$$\beta_k = \beta_i + \beta_j \quad (\text{C7})$$

If

$$Z_k = \frac{Z_i Z_j}{Z_i + Z_j}$$

Then

$$\alpha_k = \frac{\alpha_j (\alpha_i^2 + \beta_i^2) + \alpha_i (\alpha_j^2 + \beta_j^2)}{(\alpha_i + \alpha_j)^2 + (\beta_i + \beta_j)^2}$$

$$\beta_k = \frac{\beta_j (\alpha_i^2 + \beta_i^2) + \beta_i (\alpha_j^2 + \beta_j^2)}{(\alpha_i + \alpha_j)^2 + (\beta_i + \beta_j)^2} \quad (\text{C8})$$

Equations (C7) and (C8) form the basis for the feed-system impedance calculations at the frequency of interest regardless of the feed system configuration.

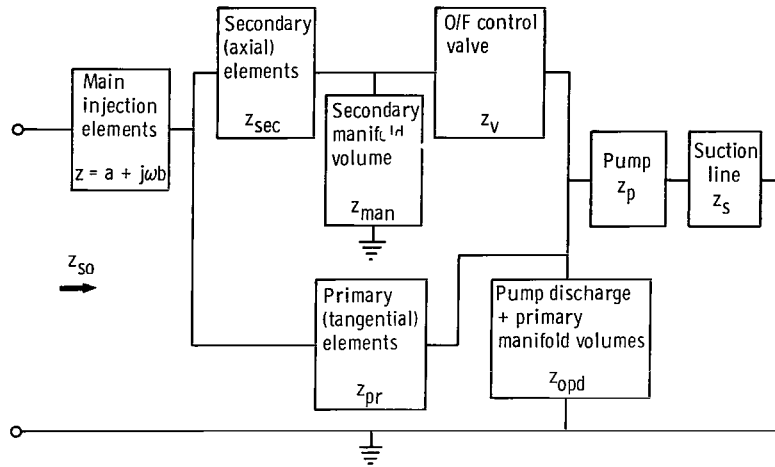


Figure 12. - Impedance representation of dual-orifice oxidizer feed system.

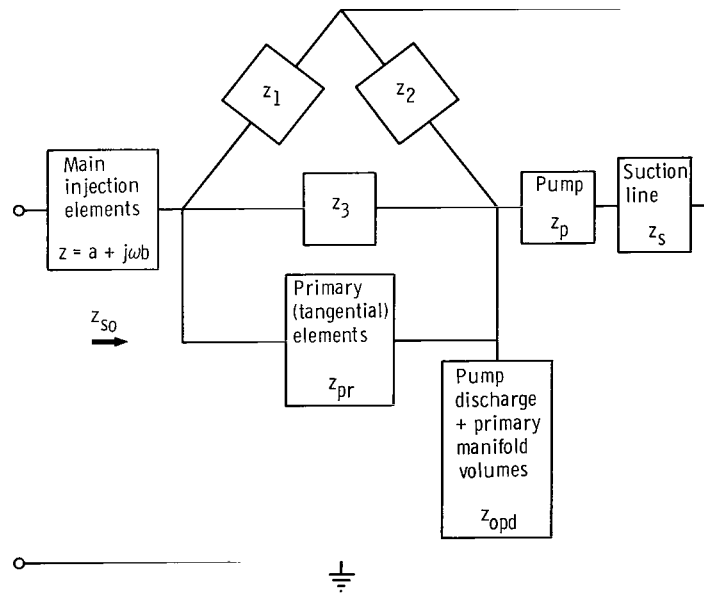


Figure 13. - Modified impedance representation of dual-orifice oxidizer feed system.

Figure 12 shows the elements for the dual-orifice oxidizer feed system. Since the stepwise reduction of the feed-system elements is based on parallel and series combinations, the tee, formed by the secondary elements, manifold, and control valve must be converted to a delta form. Figure 13 shows the modified feed system representation for the dual orifice system.

The impedances,  $Z_1$ ,  $Z_2$ , and  $Z_3$ , are evaluated from the following conversion equations:

$$Z_1 = Z_{\text{sec}} + Z_{\text{man}} + \frac{Z_{\text{sec}}Z_{\text{man}}}{Z_{\text{V}}} \quad (\text{C9})$$

$$Z_2 = Z_{\text{V}} + Z_{\text{sec}} + \frac{Z_{\text{sec}}Z_{\text{V}}}{Z_{\text{man}}} \quad (\text{C10})$$

$$Z_3 = Z_{\text{V}} + Z_{\text{man}} + \frac{Z_{\text{V}}Z_{\text{man}}}{Z_{\text{sec}}} \quad (\text{C11})$$

The stepwise reduction of the modified system is

$$Z_4 = Z_{\text{p}} + Z_{\text{S}} \quad (\text{C12})$$

$$Z_5 = \frac{Z_4 Z_{\text{opd}}}{Z_4 + Z_{\text{opd}}} \quad (\text{C13})$$

$$Z_6 = \frac{Z_5 Z_3}{Z_5 + Z_3} \quad (\text{C14})$$

$$Z_7 = \frac{Z_2 Z_{\text{pr}}}{Z_2 + Z_{\text{pr}}} \quad (\text{C15})$$

$$Z_8 = Z_6 + Z_7 \quad (\text{C16})$$

$$Z_9 = \frac{Z_1 Z_8}{Z_1 + Z_8} \quad (\text{C17})$$

$$Z_{so} = Z_g + a + j\omega b \quad (C18)$$

$$\mathcal{I}_0 = \omega b + \beta_g \quad (C19)$$

$$\mathcal{R}_0 = a + \alpha_g$$

As discussed with the single-orifice configuration, equations (C7) and (C8) were used to evaluate the various  $\alpha_i$ 's and  $\beta_i$ 's at each selected frequency.

After solutions to the characteristic equation have been found, the critical values of the real part of impedance  $\mathcal{R}'_0$  are converted to the corresponding critical values of the injection-element resistance  $a'$  using either equation (C6) or (C19).

## APPENDIX D

### COMPUTER SYMBOLS

AC	combustion chamber cross-sectional area, in. <sup>2</sup> (m <sup>2</sup> )
ACCH	storage location for critical oxidizer pressure drop ratio at operating fuel pressure-drop ratio (high frequency range)
ACCL	storage location for critical oxidizer pressure drop ratio at operating fuel pressure-drop ratio (low frequency range)
ACOUS	acoustic velocity at nozzle entrance, in. /sec (m/sec)
ACRH	storage location for critical oxidizer pressure drop ratio (high frequency range)
ACRL	storage location for critical oxidizer pressure-drop ratio (low frequency range)
AG	coefficient of second-order term in eq. (28)
AHX	imaginary part of dual orifice $Z_6$ in appendix C, sec/in. <sup>2</sup> ((N)(sec)/(m <sup>2</sup> )(kg))
AKX	imaginary part of dual orifice $Z_7$ in appendix C, sec/in. <sup>2</sup> ((N)(sec)/(m <sup>2</sup> )(kg))
ALPHA	factor under square root in eq. (28)
ALPHAG	product of angular frequency and gas residence time, rad
AOV	control valve area, in. <sup>2</sup> (m <sup>2</sup> )
AOV1	full thrust control-valve area, in. <sup>2</sup> (m <sup>2</sup> )
APF	fuel injector annulus area per element, in. <sup>2</sup> (m <sup>2</sup> )
APF0	design value of fuel annulus area per element, in. <sup>2</sup> (m <sup>2</sup> )
AT	nozzle throat area, in. <sup>2</sup> (m <sup>2</sup> )
AX	real part of single-orifice $Z_4$ or real part of dual-orifice $Z_1$ in appendix C, sec/in. <sup>2</sup> ((N)(sec)/(m <sup>2</sup> )(kg))
AXA	real part of oxidizer impedance, sec/in. <sup>2</sup> ((N)(sec)/(m <sup>2</sup> )(kg))
AYX	real part of dual-orifice $Z_7$ in appendix C, sec/in. <sup>2</sup> ((N)(sec)/(m <sup>2</sup> )(kg))
A1	cosine of phase angle due to gas-phase mixing delay
A2	cosine of phase angle due to oxidizer vaporization delay

A3	cosine of phase angle due to total oxidizer delay
BG	coefficient of first order term in eq. (28)
BO	oxidizer bulk modulus, $(N/m^2)$
BX	imaginary part of single-orifice $Z_4$ in appendix C, $sec/in.^2$ $((N)(sec)/(m^2)(kg))$
BXA	imaginary part of oxidizer impedance, $sec/in.^2$ $((N)(sec)/(m^2)(kg))$
BXI	reciprocal of imaginary part of dual orifice $Z_1$ in appendix C, $in.^2/sec$ $((m^2)(kg)/(N)(sec))$
B1	sine of phase angle due to gas-phase mixing delay
B2	sine of phase angle due to oxidizer vaporization delay
B3	sine of phase angle due to total oxidizer delay
CDF	flow coefficient of fuel-injector elements
CDO	flow coefficient of oxidizer injection orifices
CDP	flow coefficient of primary injector elements
CDS	flow coefficient of secondary injector elements
CG	coefficient of zero-order term in eq. (28)
COEFF	gas-phase delay coefficient, sec
COF	fuel-injector manifold capacitance, $in.^2 (m^2)$
COM	single-orifice injector manifold or dual-orifice secondary manifold capacitance, $in.^2 (m^2)$
COP	single-orifice oxidizer pump discharge or dual-orifice pump discharge plus primary manifold capacitance, $in.^2 (m^2)$
CSTAA	storage location for characteristic velocity, ft/sec (m/sec)
CSTAR	characteristic velocity, ft/sec (m/sec)
CX	real part of single-orifice $Z_3$ or dual-orifice $Z_8$ in appendix C, $sec/in.^2$ $((N)(sec)/(m^2)(kg))$
C1	oxidizer pump flow coefficient
C2	oxidizer pump head rise coefficient
DDX	denominator of dual orifice impedance $Z_6$ in appendix C
DENE	denominator of efficiency due to incomplete vaporization
DO	oxidizer injection orifice diameter, in. (m)

DP	primary injector element diameter, in. (m)
DPF	ratio of fuel injector pressure drop to chamber pressure at throat
DPFC	critical value of fuel-injector pressure drop to chamber pressure ratio
DPF1	critical value of fuel-injector pressure drop to chamber pressure ratio when there is more than one solution
DPF2	critical value of fuel-injector pressure drop to chamber pressure ratio when more than one solution
DPJ	oxidizer injection-orifice pressure drop, psi (N/m <sup>2</sup> )
DPO	ratio of oxidizer injection-orifice pressure drop to chamber pressure
DPOC2, 5, 8	ratios of oxidizer injection-orifice pressure drop to chamber pressure when more than one solution
DPP	pressure drop from oxidizer pump discharge to injector face, psi (N/m <sup>2</sup> )
DPS	pressure drop from oxidizer pump discharge to injection orifice input, psi (N/m <sup>2</sup> )
DS	secondary injector-element diameter, in. (m)
DSU	suction line diameter, in. (m)
DX	imaginary part of single orifice $Z_3$ or dual orifice $Z_8$ in appendix C sec/in. <sup>2</sup> ((N)(sec)/(kg)(m <sup>2</sup> ))
EC	contraction ratio
ED	element density
EFF	combustion efficiency
EFF1	storage location for combustion efficiency
ELC	cylindrical chamber length, in. (m)
ELCT	total chamber length from injector face to throat, in. (m)
ELEFF	effective length (ref. 7), in. (m)
ELGEE	generalized length (ref. 7), in. (m)
ELJ	oxidizer injection-element inductance, sec <sup>2</sup> /in. <sup>2</sup> (sec <sup>2</sup> /m <sup>2</sup> )
ELLS	suction line length, in. (m)
ELN	conical nozzle length, in. (m)
ELO	oxidizer injection-element length, in. (m)
ELSU	suction line inductance, sec <sup>2</sup> /in. <sup>2</sup> (sec <sup>2</sup> /m <sup>2</sup> )

ELSTR	characteristic length, in. (m)
ELT	chamber-nozzle geometry coefficient (ref. 8), in. (m)
ELX	real part of dual orifice impedance $Z_3$ in appendix C, $\text{sec/in.}^2$ $((N)(\text{sec})/(\text{m}^2)(\text{kg}))$
EL50	length required to vaporize 50 percent of oxidizer droplet mass, in. (m)
EMAGO	imaginary part of oxidizer impedance, $\text{sec/in.}^2$ $((N)(\text{sec})/(\text{m}^2)(\text{kg}))$
EMAGF	imaginary part of fuel impedance, $\text{sec/in.}^2$ $((N)(\text{sec})/(\text{m}^2)(\text{kg}))$
EMC	Mach number at nozzle entrance
EMR	injector momentum ratio
EMXI	reciprocal of imaginary part of dual orifice $Z_3$ (see appendix C), $\text{in.}^2/\text{sec}$ $((\text{m}^2)(\text{kg})/(N)(\text{sec}))$
ENE	number of injector elements
ENF	number of fuel elements
ENO	number of oxidizer elements
ENUM	numerator of efficiency due to incomplete vaporization
ENX	real part of dual-orifice impedance $Z_5$ (see appendix C), $\text{sec/in.}^2$ $((N)(\text{sec})/(\text{m}^2)(\text{kg}))$
ETAM	efficiency due to incomplete mixing
ETAV	efficiency due to incomplete vaporization
EX	real part of single-orifice $Z_2$ or dual-orifice $Z_9$ (see appendix C), $\text{sec/in.}^2$ $((N)(\text{sec})/(\text{m}^2)(\text{kg}))$
FFH	storage location for frequency at critical oxidizer pressure-drop ratio, operating fuel pressure-drop ratio (high-frequency range), Hz
FFL	storage location for frequency at critical oxidizer pressure-drop ratio, operating fuel pressure-drop ratio (low-frequency range), Hz
FG	partial derivative of chamber pressure with respect to fuel flow, $\text{sec/in.}^2$ $((N)(\text{sec})/(\text{m}^2)(\text{kg}))$
FH	storage location for frequency at critical injector pressure-drop ratios (high-frequency range), Hz
FL	storage location for frequency at critical injector pressure-drop ratios (low-frequency range), Hz
FOP	fraction of oxidizer flow through primary (tangential) injector elements

FREQ	frequency, Hz
FX	imaginary part of single orifice $Z_2$ or dual orifice $Z_9$ (see appendix C), sec/in. <sup>2</sup> ((N)(sec)/(m <sup>2</sup> )(kg))
GAM	input value of specific heat ratio for combustion products
GAMMA	specific heat ratio of combustion products
G	acceleration due to gravity, ft/sec (m/sec)
GC	gravitational constant, 32.2 ((lbm)(ft)/(lbf)(sec <sup>2</sup> )) (1 (kg)(m)/(N)(sec <sup>2</sup> ))
GX	real part of dual orifice impedance $Z_6$ (see appendix C), sec/in. <sup>2</sup> ((N)(sec)/(m <sup>2</sup> )(kg))
HV	oxidizer heat of vaporization, Btu/lbm (J/kg)
HVT	heat of vaporization coefficient (ref. 8)
I	throttling index
II	multiple oxidizer solution index
IL	high-frequency solution ordering index
IM	multiple solution frequency index
IX	low-frequency solution ordering index
IX1	low-frequency solution order index
IZ	variable fuel-area solution order index
J	calculation counting index
JJ	type of study index
JM	existence of high-frequency solution index
JN	existence of low-frequency solution index
JX	low-frequency solution ordering index
K	variable fuel-area index
KK	high-frequency solution ordering index
KX1	high-frequency solution ordering index
L	solution ordering index
LI	low-frequency solution ordering index
LJ	high-frequency solution ordering index
LX	high-frequency solution ordering index

MM	type of injector index
MN	lower throttling limit index
N	number of boundary points
ND	number of solution points in set
NE	one more than number of boundary points
NN	frequency band index
NS	one less than number of low-frequency boundary points
N1	number of low-frequency boundary points
N2	number of high-frequency boundary points
N11	one less than number of low-frequency boundary points
N22	one less than number of high-frequency boundary points
OF	mixture ratio
OX	imaginary part of dual orifice $Z_5$ in appendix C, $\text{sec/in.}^2 ((N)(\text{sec})/(\text{kg})(\text{m}^2))$
PC	total chamber pressure at nozzle entrance, $\text{psi } (N/\text{m}^2)$
PCI	total chamber pressure at injector face, $\text{psi } (N/\text{m}^2)$
PC1	full thrust total chamber pressure at nozzle entrance, $\text{psi } (N/\text{m}^2)$
PF	fuel-injector manifold pressure, $\text{psi } (N/\text{m}^2)$
PO	oxidizer pump discharge pressure, $\text{psi } (N/\text{m}^2)$
PS	oxidizer pump inlet pressure, $\text{psi } (N/\text{m}^2)$
PSUP	pressure feeding secondary (axial) injector elements, $\text{psi } (N/\text{m}^2)$
PV	percent vaporized with chamber, nozzle
PX	real part of dual orifice $Z_2$ (see appendix C), $\text{sec/in.}^2 ((N)(\text{sec})/(\text{kg})(\text{m}^2))$
QX	imaginary part of dual orifice $Z_2$ (see appendix C), $\text{sec/in.}^2 ((N)(\text{sec})/(\text{kg})(\text{m}^2))$
RC	combustion products gas constant, $\text{ft}^{\circ}\text{R } (m/K)$
RESF	linearized fuel
RESOB	linearized secondary-element resistance, $\text{sec/in.}^2 ((N)(\text{sec})/(\text{kg})(\text{m}^2))$
RESOJ	linearized oxidizer injection-orifice resistance, $\text{sec/in.}^2 ((N)(\text{sec})/(\text{kg})(\text{m}^2))$
RESOP	linearized oxidizer pump resistance, $\text{sec/in.}^2 ((N)(\text{sec})/(\text{kg})(\text{m}^2))$

RESOS	linearized single-orifice valve resistance or dual-orifice primary element resistance, $\text{sec/in.}^2 ((\text{N})(\text{sec})/(\text{kg})(\text{m}^2))$
RESOV	linearized dual-orifice valve resistance, $\text{sec/in.}^2 ((\text{N})(\text{sec})/(\text{kg})(\text{m}^2))$
RF	fuel gas constant, $\text{ft}/^\circ\text{R}$ (m/K)
RHO	oxidizer mass density, $\text{lbm/in.}^3$ ( $\text{kg}/\text{m}^3$ )
RMCTN	mean oxidizer drop radius, in. (m)
RPC	critical value of real part of oxidizer injection-orifice impedance (one solution), $\text{sec/in.}^2 ((\text{N})(\text{sec})/(\text{kg})(\text{m}^2))$
RPC1, 2	critical values of real part of oxidizer injection-orifice impedance (multiple solutions), $\text{sec/in.}^2 ((\text{N})(\text{sec})/(\text{kg})(\text{m}^2))$
RRF	critical value of real part of fuel-injector impedance (one solution), $\text{sec/in.}^2 ((\text{N})(\text{sec})/(\text{kg})(\text{m}^2))$
RRF1, 2	critical values real part of fuel-injector impedance (multiple solutions), $\text{sec/in.}^2 ((\text{N})(\text{sec})/(\text{kg})(\text{m}^2))$
RX	critical value of real part of oxidizer feed-system impedance (one solution), $\text{sec/in.}^2 ((\text{N})(\text{sec})/(\text{kg})(\text{m}^2))$
RX1, 2	critical values of real part of oxidizer feed-system impedance (multiple solutions), $\text{sec/in.}^2 ((\text{N})(\text{sec})/(\text{kg})(\text{m}^2))$
S	nozzle shape factor (ref. 8)
SLOPA	storage location for partial derivative of characteristic velocity with respect to mixture ratio, $\text{ft}/\text{sec}$ (m/sec)
SLOPE	partial derivative of characteristic velocity with respect to mixture ratio, $\text{ft}/\text{sec}$ (m/sec)
SPEED	oxidizer pump speed, rpm
ST	oxidizer surface tension, $\text{dyne}/\text{cm}$ (N/m)
SWC	correction factor for swirler
TAUM	gas-phase mixing and reaction time delay, sec
TAUT	total oxidizer time delay, sec
TAUV	oxidizer vaporization time delay, sec
TC	combustion temperature, $^\circ\text{R}$ (K)
TEMP	temporary storage location for ordering solutions
TF	fuel temperature, $^\circ\text{R}$ (K)

TF1	full thrust fuel temperature, °R (K)
THETAG	gas residence time, sec
THETAM	angle due to gas-phase mixing delay, rad
THETAV	angle due to oxidizer vaporization delay, rad
TK	input value of combustion temperature, K
TPE	thrust per element, lbf (N)
TT	temperature coefficient (ref. 8)
UF	unit correction factor, 12 in./ft (1 m/m)
UPH	storage location for high-frequency solution of critical fuel-injector pressure drop-ratio
UPL	storage location for low-frequency solution of critical fuel-injector pressure-drop ratio
UPPH	storage location for ordered values of operating fuel-injector pressure-drop ratio (high-frequency range)
UPPL	storage location for ordered values of operating fuel-injector pressure-drop ratio (low-frequency range)
VC	cylindrical chamber volume, in. <sup>3</sup> (m <sup>3</sup> )
VELC	gas velocity at nozzle entrance, in./sec (m/sec)
VF	fuel-injection velocity, in./sec (m/sec)
VIS	oxidizer viscosity, cp ((N)(sec)/m <sup>2</sup> )
VN	conical nozzle volume, in. <sup>3</sup> (m <sup>3</sup> )
VOF	fuel-injector manifold volume, in. <sup>3</sup> (m <sup>3</sup> )
VOM	single-orifice manifold or dual-orifice secondary manifold volume, in. <sup>3</sup> (m <sup>3</sup> )
VORTC	ratio of secondary (axial) to total oxidizer flow
VOS	single-orifice pump discharge or dual-orifice pump discharge plus primary manifold volume, in. <sup>3</sup> (m <sup>3</sup> )
W	angular frequency, rad/sec
WF	fuel flow rate, lbm/sec (kg/sec)
WF1	full thrust fuel flow rate, lbm/sec (kg/sec)
WO	oxidizer flow rate, lbm/sec (kg/sec)

WOP primary (tangential) flow rate, lbm/sec (kg/sec)  
 WOS secondary (axial) flow rate, lbm/sec (kg/sec)  
 WOSV secondary flow specified by vortex characteristic, lbm/sec (kg/sec)  
 WO1 full thrust oxidizer flow rate, lbm/sec (kg/sec)  
 WT input value of molecular weight of combustion products, lbm/(lb)(mole)  
 (g/(g)(mole))  
 WTO oxidizer molecular weight, lbm/(lb)(mole) (g/(g)(mole))  
 WTOT total propellant flow rate, lbm/sec (kg/sec)  
 WTT molecular weight coefficient (ref. 8)  
 X throttling index  
 XG partial derivative of chamber pressure with respect to oxidizer flow,  $\text{sec/in.}^2$   
 ((N)(sec)/(kg)(m<sup>2</sup>))  
 XP primary-element pressure-drop coefficient,  $\text{in.}^{-2}$  (m<sup>-2</sup>)  
 XS secondary-element pressure-drop coefficient,  $\text{in.}^{-2}$  (m<sup>-2</sup>)  
 Y substituted parameter in solution of eq. (28)  
 YY variable fuel-area index

# APPENDIX E

## COMPUTER LISTINGS FOR DIGITAL CHUGGING ANALYSIS

### MAIN PROGRAM

```
COMMON /ABC/ W,COM,RESOP,COP,ELJ,RESOJ,W0,PC
DIMENSION GAM(2), TK(2), WT(2)
DIMENSION UPL(100), ACRL(100), UPH(100), ACRH(100), FL(100), FH(10)
10)
DIMENSION ACCL(10), UPPL(10), FFL(10), ACCH(10), UPPH(10), FFH(10)
C READ IN AND WRITE VALUES OF SPECIFIC HEAT RATIO, COMBUSTION TEMP.,
C AND MOLECULAR WT. OF PRODUCTS AT TWO CHAMBER PRESSURES FOR NOMINAL
C MIXTURE RATIO. FOR THIS CASE N=1 IS FOR PC=800 AND N=2 IS FOR PC
C = 500
  READ (5,1) (GAM(N),TK(N),WT(N),N=1,2)
  WRITE (6,1) (GAM(N),TK(N),WT(N),N=1,2)
1  FORMAT (6X, F6.4, 1X, F5.0, 1X, F6.3, 1X, F6.4, 1X, F5.0, 1X, F6.3)
C MM=0 DENOTES DUAL ORIFICE
C MM=1 DENOTES SINGLE ORIFICE
  MM=0
  GC=32.2
  UF=12.
  G=32.2
C THE FOLLOWING DATA IS FOR METHANE
  RF=12.*90.37
C THE FOLLOWING DATA IS FOR 82.6 PERCENT FLOX
  TCR=261.
  WTD=36.8
  HV=78.0
  RHO=.0538
  BD=7.84E+4
  ST=67.0
  VIS=.22
  RSTVC=(( .0411/RHO)* (ST/13.2)* (VIS/.19) )**.25
  WTI=(WTD/100.)**.35
  HVT=(HV/140.)**.8
C THE FOLLOWING COEFFICIENTS ARE SUPPLIED FOR OXIDIZER PUMP. C1 IS
C A FLOW COEFFICIENT AND C2 IS A HEAD RISE COEFFICIENT
  C1=44.253
  C2=3.253E-6
C THE FOLLOWING ARE FULL THRUST OPERATING CONDITIONS
  IF (MM.EQ.0) GO TO 2
  PC1=500.
  OF=5.25
  W01=10.31
  WF1=W01/OF
  TF1=1373.
  T0=165.
  PS=40.
  GO TO 3
2  PC1=500.
  OF=5.25
  W01=10.46
  WF1=W01/OF
```

```

TF1=1344.
T0=156.5
PS=40.
C THE FOLLOWING IS GEOMETRY DATA. A CONICAL NOZZLE IS ASSUMED AND
C ITS LENGTH IS BASED ON SPECIFIED CHARACTERISTIC LENGTH AND
C CONTRACTION RATIO AND THROAT AREA
3 IF (MM.EQ.0) GO TO 4
  AT=5.309
  EC=4.
  ELSTR=37.
  ELCT=13.
  GO TO 5
4 AT=5.336
  EC=4.
  ELSTR=40.
  ELCT=13.
5 ELN=3.*(ELSTR-ELCT*EC)/(1.-2.*EC+EC**.5)
  ELC=ELCT-ELN
  VN=AT*ELN*(1.+EC+EC**.5)/3.
  AC=AT*EC
  VC=AC*ELC
  S=VN/AC/ELN
  ELT=ELC/EC**.44+.83*ELN/S**.33/EC**.22
C THE FOLLOWING IS SPECIFIED INJECTOR GEOMETRY
  IF (MM.EQ.0) GO TO 6
  DD=.0694
  ELD=.694
  ENF=63.
  GO TO 7
6 DP=.01403
  DS=.0920
  DD=.0846
  ENF=68.
  ELD=1.
7 FC=ENE/AC
  FND=ENF
  ENF=ENE
C FOR DUAL ORIFICE INJECTOR, VOM IS MANIFOLD VOLUME FOR SECONDARY FLOW
C AND VOS IS SUM OF MANIFOLD VOLUME FOR PRIMARY FLOW AND VOLUME BETWEEN
C PUMP AND INJECTOR. FOR SINGLE ORIFICE INJECTOR, VOM IS INJECTOR
C MANIFOLD VOLUME, VOS IS VOLUME BETWEEN PUMP AND INJECTOR
C VOF IS FUEL MANIFOLD VOLUME
  IF (MM.EQ.0) GO TO 8
  VDF=4.
  FLLS=18.
  DSU=2.5
  VOS=50.
  VOM=21.
  AOV1=.229
  CDD=.6
  CCP=.6
  CDS=.6
  CDF=.6
  SWC=.448
  APFO=1.158E-2
  GO TO 9
8 AOV1=.215
  CDD=.6
  CCP=.6

```

```

CDS=.6
CDF=.4247
SWC=.448
VOF=4.
ELLS=18.
DSU=2.5
VOS=50.
VOM=21.
APFO=1.0535E-2
C AT THIS POINT THE DECISION IS MADE WHETHER TO GENERATE BOUNDARIES
C AT VARIOUS CHAMBER PRESSURES, USING OPERATING POINT DELAYS OR TO
C GENERATE BOUNDARIES USING DELAY VALUES SENSITIVE TO FUEL ANNUALS
C AREA. JJ=0 DENOTES FORMER, JJ=1 DENOTES LATTER
9 J=1
  JJ=1
  MN=1
  LI=0
  II=0
  IF (JJ.EQ.0) MN=10
  DO 89 I=1,MN
  X=I
  PC=PC1*(1.1-X*.1)
  K=0
  APF=APFO
C SPECIFY FUEL TEMPERATURE AND CONTROL VALVE RELATIONSHIPS TO
C CHAMBER PRESSURE
  TF=TF1*(PC1/PC)**.116
  ANV=A1V1*(-.00977+1.035*(PC/PC1)-.0252*(PC/PC1)**2)
C COMPUTE THEORETICAL CHARACTERISTIC VELOCITY AT GIVEN CHAMBER PRESSURE
C AND MIXTURE RATIO ALSO PARTIAL W.R.T. MIXTURE RATIO
  CALL CSTRR (PC,OF,CSTAR,SLOPE)
C AT FULL THRUST, FLOWS ARE AS SPECIFIED. AT THROTTLED CONDITIONS
C (J NOT EQUAL TO 1), FLOWS BASED ON PREVIOUSLY COMPUTED
C EFFICIENCY.
  IF (J.EQ.1) GO TO 10
  GO TO 11
10 WD=WD1
  WF=WF1
  GO TO 12
11 EFF=EFF1
  WTOT=PC*AT*GC/CSTAR/EFF
  WD=OF/(OF+1.)*WTOT
  WF=WD/OF
  GO TO 13
C AT FULL THRUST, COMPUTE EFFICIENCY
12 EFF=PC*AT*GC/CSTAR/(WD+WF)
C INTERPOLATE OR EXTRAPOLATE LINEARLY TO DETERMINE SPECIFIC HEAT
C RATIO, MOLECULAR WEIGHT AND COMBUSTION TEMPERATURE. USE RESULTS
C TO CALCULATE CHAMBER PRESSURE AT INJECTOR FACE.
13 GAMMA=GAM(2)+(GAM(1)-GAM(2))*(PC-500.)/300.
  TC=1.8*(TK(2)+(TK(1)-TK(2))*(PC-500.)/300.)
  RC=1544./(WT(2)+(WT(1)-WT(2))*(PC-500.)/300.)
  ACOUS=SQRT(GC*GAMMA*RC*TC)*UF
  EXP=(GAMMA+1.)/(GAMMA-1.)/2.
  EMC=(1./(1.+(GAMMA-1.)/2.))*EXP/EC
  VELC=EMC*ACOUS
  EXP1=GAMMA/(GAMMA-1.)
  PCI=PC*(1.+GAMMA*EMC**2)/(1.+(GAMMA-1.)/2.*EMC**2)**EXP1
C COMPUTE VELOCITIES AND PRESSURE DROPS

```

```

14  VF=WF/ENF/PCI*RF*TF/APF
    PF=PCI*SQRT(1.+VF**2/CDP**2/RF/TF/GC/UF)
    VU=WQ/END/RHO/3.1416/DO**2*4.
    EMR=VF/VU/OF
    DPJ=(WQ/END/CDP/3.1416/DO**2*4.)**2/RHO/2./GC/UF
    IF (MM.EQ.0) GO TO 15
    DPS=(WQ/AUV)**2/RHO/2./GC/UF
    DPP=DPJ+DPS
    PG=PCI+DPP
    GO TO 17
15  XS=4./END/CDP/3.1416/DS**2
    XP=4./END/3./CDP/3.1416/DP**2
    WOP=WQ/(1.+XP/(1./AUV**2+XS**2)**.5)
    WOS=WQ-WOP
    FOP=WOP/WQ
    PSUP=PCI+DPJ+(WOS*XS)**2/RHO/2./GC/UF
    DPS=(WOP*XP)**2/RHO/2./GC/UF
    DPP=DPJ+DPS
    PO=PCI+DPP
    VORTC=-2.45*(PO/PSUP)**2+4.52*(PO/PSUP)-1.1259
    WOSV=WQ*VORTC
    IF (ABS(WOSV-WOS).GT..01) GO TO 16
    GO TO 17
16  DS=DS*(WOSV/WOS)**.5
    GO TO 15
C   THE FOLLOWING SECTION COMPUTES DROP SIZE, BURNING LENGTH,
C   EFFECTIVE LENGTH, DELAY TIMES, PERCENT VAPORIZED AND
C   PERFORMANCE LOSS DUE TO INCOMPLETE VAPORIZATION. AT FULL THRUST,
C   THE PERFORMANCE LOSS DUE TO INCOMPLETE MIXING IS INFERRED. AT
C   THROTTLED CONDITION, OVERALL EFFICIENCY IS CALCULATED AND COMPARED
C   WITH THE VALUE USED. IF ERROR EXISTS, FLOWS ARE ADJUSTED
17  RMCTN=.5*.236*RS*TV*SWC*DO*SQRT(OF*VO/VF)
    TT=(1.-TO/TCR)**.4
    EL50=2.75*EC**.44*TT*(RMCTN/.003)**1.45*(VO/1200.)**.75*WTT*HVT/(P
1C/300.)**.66
    FLEFF=ELT/EL50*2.75*EC**.44*WTT*HVT
    TAUV=EL50/VO
    ELGEE=ELEFF/WTT/HVT
    PV=PP/(ELGEE)
    DENE=CSTAR*(OF+1.)
    CALL CSTRK (PC,PV*OF,CSTAA,SLOPA)
    FNUM=CSTAA*(PV*OF+1.)
    ETAV=FNUM/DENE
    IF (J.GT.1) GO TO 18
    ETAM=EFF/ETAV
    GO TO 20
18  EFF=ETAV*ETAM
    IF (ABS(EFF1-EFF).GT..001) GO TO 19
    GO TO 20
19  WTOT=WQ+WF
    WTOT=WTOT*EFF1/EFF
    WQ=OF/(OF+1.)*WTOT
    WF=WQ/OF
    EFF1=EFF
    GO TO 14
C   COMPUTE GAS RESIDENCE TIME, THRUST PER ELEMENT, GAS PHASE DELAY
C   COEFFICIENT AND OPERATING POINT PRESSURE DROP RATIOS
20  THETAG=EFF*CSTAR*ELSTR/GAMMA/RC/TC/386.
    TPE=10.*PC/ENE

```

```

DPU=DPJ/PC
DPF=(PF-PCI)/PC
COEFF=1.E+3*(ELC+ELN-EL50)/VELC
TAUM=FM(COEFF)
TAUT=TAUM+TAUV

```

C THE FOLLOWING SECTION COMPUTES LINEARIZED RESISTANCES, INDUCTANCES,  
C CAPACITANCES AND GAINS.

```

XG=(CSTAR+(OF+1.)*SLOPE)/AT/GC*EFF*PCI/PC
FG=(CSTAR-OF*(OF+1.)*SLOPE)/AT/GC*EFF*PCI/PC
RESF=(PF**2-PCI**2)/WF/PCI
RESQJ=2.*(DPP-DPS)/WO
CALL RESXP (C1,C2,RHO,WO,PS,PO,SPEED,RESOP)
RESQS=2.*DPS/WO
ELJ=ELD*4./END/3.1416/DO**2/UF/G
ELSU=FLLS*4./3.1416/DSU**2/UF/G
COP=RHO*VDS/BO*G/GC
COM=RHO*VCM/BO*G/GC
COF=VDF/RF/TF

```

C AT THIS POINT, PARAMETERS OF INTEREST ARE WRITTEN OUT.

```

WRITE (6,21)
21  FORMAT (2X,2HPC,4X,2HED,2X,2HNE,4X,2HNO,4X,3HF/E,5X,2HDO,6X,4HAF/E
1,6X,2HC*.6X,2HL*,5X,3HEFF,4X,2HWG,6X,2HWF,4X,2HVO,8X,2HPS,5X,2HMC,
25X,3HPCI,3X,6HTHETAG)
WRITE (6,22) PC,ED,ENE,END,TPE,DO,APF,CSTAR,ELSTR,EFF,WO,DF,VO,PS,
1FMC,PCI,THETAG
22  FORMAT (1X,F5.1,2X,F2.0,2X,F3.0,2X,F4.0,2X,F5.1,2X,F5.4,2X,E9.4,2X
1,F6.1,3X,F4.1,3X,F4.3,3X,F5.2,2X,F5.2,2X,F6.1,2X,F7.1,2X,F4.3,2X,F
25.1,2X,1PE9.3)
WRITE (6,23)
23  FORMAT (3X,2HPO,6X,2HPF,5X,3HDPF,5X,3HDPO,4X,3HL50,4X,3HLEF,2X,4HL
1GFN,3X,2HPV,6X,4HTAUT,4X,5HTEMP,3X,3HMOR,4X,2HDP,4X,4HTAJM,14X,2H
2DS,6X,4HETAM)
WRITE (6,24) PO,PF,DPF,DPU,EL50,ELEFF,ELGEE,PV,TAUT,TF,EMR,DP,TAUM
1,DS,FTAM
24  FORMAT (1X,F6.1,2X,F6.1,1X,F6.4,2X,F5.4,3X,F5.3,1X,F5.1,2X,F4.1,2X
1,F4.3,2X,1PE9.3,2X,OPF5.0,1X,F6.3,2X,F5.4,2X,1PE9.3,8X,OPF5.4,4X,F
24.3)
WRITE (6,25)
25  FORMAT (3X,3HWOP,7X,6HWOP/WO,4X,3HAOV,6X,6HOXGAIN,4X,3HFJELGAIN,3X
1,7HSPFEJX,4X,8HOXINJUPR,4X,10HOXSPLITUPR,3X,9HOXPUMPRES,4X,8HOXIN
2JIND,4X,6HOXSCAP,5X,6HOXMCAP)
WRITE (6,26) WOP,FOP,AOV,XG,FG,SPEED,DPJ,DPS,RESOP,ELJ,COP,COM
26  FORMAT (2X,F6.3,4X,F6.4,4X,F6.4,4X,F6.3,4X,F6.3,4X,1PE9.3,3X,1PE9.
13,3X,1PE9.3,4X,1PE9.3,3X,1PE9.3,2X,1PE9.3,1X,1PE9.3//)
FFF1=FFF
IF ((1.LT.MN).AND.(JJ.EQ.1)) GO TO 88
IF ((K.EQ.0).AND.(JJ.EQ.1)) GO TO 79

```

C AT THIS POINT THE FREQUENCY BANDS AND INCREMENT ARE SELECTED AND  
C THE SOLUTION OF THE CHARACTERISTIC EQUATION IS INITIATED

```

FREQ=74.9
JN=0
N=0
NN=0
27  FREQ=FREQ+.1
IF ((FREQ.GT.300.).AND.(FREQ.LT.400.)) GO TO 28
GO TO 29
28  IF (N.EQ.0) JN=1
N1=N
FREQ=400.

```

```

JM=0
N=0
NN=1
GO TO 30
29 IF (FREQ.GT.650.) GO TO 50
30 W=6.2832*FREQ
    I I=1
    RX=0.
    RX1=0.
    RX2=0.
    RRF=0.
    RRF1=0.
    RRF2=0.
    DPOC2=0.
    DPOC5=0.
    DPOC8=0.
    DPFC=0.
    DPF1=0.
    DPF2=0.
C AT THIS POINT TERMS IN THE CHARACTERISTIC EQUATION ARE EVALUATED
C AT SPECIFIED FREQUENCY
    EMAGF=-1./W/CJF*PF/PCI
    THETAT=TAUT*W
    THETAM=TAUM*W
    THETAV=TAUV*W
    THETAL=FLJ*W
    ALPHAG=THETAG*W
    A1=COS(THETAM)
    B1=SIN(THETAM)
    A2=COS(THETAV)
    B2=SIN(THETAV)
    A3=COS(THETAT)
    B3=SIN(THETAT)
    Y=B1+ALPHAG*A1
C AT THIS POINT THE SECOND AND FIRST ORDER COEFFICIENTS IN THE
C QUADRATIC EQUATION FOR CRITICAL QX REAL PART ARE EVALUATED
    AG=Y-EMAGF/FG*(1.+ALPHAG**2)
    BG=-XG*B2-2.*XG*EMAGF/FG*(A3-ALPHAG*B3)
    IF (MM.EQ.0) GO TO 31
C THE FOLLOWING SECTION COMPUTES THE REAL AND IMAGINARY PARTS OF
C THE IMPEDANCE LOOKING UPSTREAM FOR A SINGLE ORIFICE CONFIGURATION
    RESOS=2.*DPS/WO
    DDX=(W*RESUP*COP)**2+1.+W**4*ELSU**2*COP**2-2.*W**2*ELSJ*COP
    FX=(-W*COP*RESOP**2+W*ELSU-W**3*COP*ELSU**2)/(DDX)
    EX=RESOP/DDX
    DX=FX
    CX=RESOS+EX
    BX=(-W*COM*(CX**2+DX**2)+DX)/((W*COM*CX)**2+(W*COM*DX-1.)**2)
    AX=CX/((W*COM*CX)**2+(W*COM*DX-1.)**2)
    AXA=AX
    BXA=BX
    GO TO 32
31 CONTINUE
C THE FOLLOWING SECTION COMPUTES THE REAL AND IMAGINARY PARTS OF THE
C IMPEDANCE LOOKING UPSTREAM FOR A DUAL ORIFICE CONFIGURATION
    RESOS=2.*DPS/WOP
    RESOV=2.*(WOS/AOV)**2/772./RHO/WOS
    RESUB=2.*(DPS-(WOS/AOV)**2/772./RHO)/WOS
    QX=W*RESUB*RESOV*COM

```

```

PX=RESOV+RESOB
UDX=(W*RESOP*COP)**2+1.+W**4*ELSU**2*COP**2-2.*W**2*ELSJ*COP
UX=(-W*COP*RESOP**2+W*ELSU-W**3*COP*ELSU**2)/(DDX)
ENX=RFSOP/DDX
EMXI=-W*RESOB*COM/(RESOV+RESOB)
FLX=RFSOV
AX=RESOB
BXI=-W*RESOV*COM/(RESOV+RESOB)
AKX=UX*RESOS**2/((RESOS+PX)**2+OX**2)
AHX=(. )X*((ELX*EMXI)**2+1.)+EMXI*(ENX**2+OX**2)/(EMXI**2*(ELX+ENX)
1**2+(1.+OX*EMXI)**2)
AYX=(PX*RESOS**2+RESOS*(PX**2+OX**2))/((RESOS+PX)**2+OX**2)
GX=(ENX*((ELX*EMXI)**2+1.)+ELX*EMXI**2*(ENX**2+OX**2))/(EMXI**2*(E
1LX+ENX)**2+(1.+OX*EMXI)**2)
DX=AHX+AKX
CX=GX+AYX
EX=(CX*((AX*BXI)**2+1.)+AX*BXI**2*(CX**2+DX**2))/(BXI**2*(AX+CX)**
12+(1.+DX*BXI)**2)
FX=(DX*((AX*BXI)**2+1.)+BXI*(CX**2+DX**2))/(BXI**2*(AX+CX)**2+(1.+
1DX*BXI)**2)
AXA=EX
BXA=FX

```

32 EMAG0=THETAL+BXA

C AT THIS POINT THE ZEROth ORDER COEFFICIENT IN THE QUADRATIC  
C EQUATION FOR CRITICAL OX REAL PART IS EVALUATED. THE FOLLOWING  
C SFCTION SOLVES THE QUADRATIC AND RELATES SOLUTION TO THE  
C PRESSURE DROP RATIO

```

CG=EMAG0**2*Y-EMAG0*XG*A2+2.*XG*EMAGF*EMAG0/FG*(B3+ALPHAG*A3)-EMAG
1F*EMAG0**2/FG*(1.+ALPHAG**2)-XG**2*EMAGF/FG

```

```

IF (AG.NE.0.) GO TO 33

```

```

RX=-CG/BG

```

```

RPC=RX-AXA

```

```

IF (RPC.LE.0.) GO TO 27

```

```

DPOC2=RPC*W0/PC/2.

```

```

GO TO 38

```

33 ALPHA=BG\*\*2-4.\*AG\*CG

```

IF (ALPHA) 27,34,35

```

34 RX=-BG/2./AG

```

RPC=RX-AXA

```

```

IF (RPC.LE.0.) GO TO 27

```

```

DPOC2=RPC*W0/PC/2.

```

```

GO TO 38

```

35 RX1=(-BG+SQRT(ALPHA))/2./AG

```

RX2=(-BG-SQRT(ALPHA))/2./AG

```

```

RPC1=RX1-AXA

```

```

RPC2=RX2-AXA

```

```

IF ((RPC1.LE.0.).AND.(RPC2.LE.0.)) GO TO 27

```

```

IF (RPC1.LE.0.) GO TO 36

```

```

IF (RPC2.LE.0.) GO TO 37

```

```

II=2

```

```

DPOC5=RPC1*W0/PC/2.

```

```

DPOC8=RPC2*W0/PC/2.

```

```

GO TO 39

```

36 RPC=RPC2

```

DPOC2=RPC*W0/PC/2.

```

```

RX=RX2

```

```

GO TO 38

```

37 RPC=RPC1

```

DPOC2=RPC*W0/PC/2.

```

```

GO TO 38
C AT THIS POINT THE CRITICAL FUEL REAL PART IS DETERMINED USING
C UX SOLUTIONS. THE RESULT IS RELATED TO THE PRESSURE DROP RATIO
38 RRF=(FG*RX*B1-FG*EMAGO*A1-XG*EMAGF*A3+ALPHAG*EMAGO*EMAGF-EMAGF*RX)
1/(RX*ALPHAG+EMAGO-XG*B3)
IF (RRF) 27,27,43
39 RRF1=(FG*RX1*B1-FG*EMAGO*A1-XG*EMAGF*A3+ALPHAG*EMAGO*EMAGF-EMAGF*RX1)
/(RX1*ALPHAG+EMAGO-XG*B3)
RRF2=(FG*RX2*B1-FG*EMAGO*A1-XG*EMAGF*A3+ALPHAG*EMAGO*EMAGF-EMAGF*RX2)
/(RX2*ALPHAG+EMAGO-XG*B3)
IF (RRF1.GT.C.) GO TO 40
RRF1=0.
DPOC5=0.
IF (RRF2.LE.C.) GO TO 41
GO TO 42
40 IF (RRF2.GT.C.) GO TO 42
41 RRF2=0.
DPOC8=0.
42 DPF1=SQRT(PCI**2+WF*PCI*RRF1)/PC-PCI/PC
DPF2=SQRT(PCI**2+WF*PCI*RRF2)/PC-PCI/PC
GO TO 44
43 DPF3=SQRT(PCI**2+WF*PCI*RRF)/PC-PCI/PC
44 IF ((DPOC2.EQ.0.).AND.(DPF3.EQ.0.).AND.(DPOC5.EQ.0.).AND.(DPF1.EQ.
10.).AND.(DPOC8.EQ.0.).AND.(DPF2.EQ.0.)) GO TO 27
C AT THIS POINT THE LOW AND HIGH FREQUENCY SOLUTIONS ARE SORTED
C IN ORDER OF INCREASING FUEL PRESSURE DROP RATIO
IF (NN.EQ.1) GO TO 47
IF (DPF1.EQ.0.) GO TO 45
IF (DPF2.EQ.C.) GO TO 46
N=N+1
UPL(N)=DPF1
FL(N)=FRFQ
ACRL(N)=DPOC5
N=N+1
UPL(N)=DPF2
FL(N)=FREQ
ACRL(N)=DPOC8
GO TO 27
45 N=N+1
UPL(N)=DPF2
FL(N)=FREQ
ACRL(N)=DPOC8
GO TO 27
46 N=N+1
UPL(N)=DPF1
FL(N)=FREQ
ACRL(N)=DPOC5
GO TO 27
47 IF (DPF1.EQ.0.) GO TO 48
IF (DPF2.EQ.C.) GO TO 49
N=N+1
UPH(N)=DPF1
FH(N)=FREQ
ACRH(N)=DPOC5
N=N+1
UPH(N)=DPF2
FH(N)=FRFQ
ACRH(N)=DPOC8
GO TO 27

```

```

48  N=N+1
    UPH(N)=DPF2
    FH(N)=FREQ
    ACRH(N)=DPOC8
    GO TO 27
49  N=N+1
    UPH(N)=DPF1
    FH(N)=FREQ
    ACRH(N)=DPOC5
    GO TO 27
50  IF ((FREQ.GT.650.).AND.(N.EQ.0)) JM=1
    N2=N
    IF ((JN.EQ.1).AND.(JM.EQ.1)) GO TO 78
    IF (JM.EQ.1) GO TO 51
    IF (JN.EQ.1) GO TO 52
    IM=3
    GO TO 53
51  IM=1
    GO TO 53
52  IM=2
    GO TO 56
53  N11=N1-1
    DO 55 IX=1,N11
    IX1=IX+1
    DO 55 JX=IX1,N1
    IF (UPL(IX)-UPL(JX)) 55,55,54
54  TEMP=UPL(IX)
    UPL(IX)=UPL(JX)
    UPL(JX)=TEMP
    TEMP=ACRL(IX)
    ACRL(IX)=ACRL(JX)
    ACRL(JX)=TEMP
    TEMP=FL(IX)
    FL(IX)=FL(JX)
    FL(JX)=TEMP
55  CONTINUE
    IF (IM.EQ.1) GO TO 59
56  N22=N2-1
    DO 58 KX=1,N22
    KX1=KX+1
    DO 58 LX=KX1,N2
    IF (UPH(KX)-UPH(LX)) 58,58,57
57  TEMP=UPH(KX)
    UPH(KX)=UPH(LX)
    UPH(LX)=TEMP
    TEMP=ACRH(KX)
    ACRH(KX)=ACRH(LX)
    ACRH(LX)=TEMP
    TEMP=FH(KX)
    FH(KX)=FH(LX)
    FH(LX)=TEMP
58  CONTINUE
C AT THIS POINT, THE VARIABLE AREA CASE(JJ=1) CALLS FOR INTERPOLATION
C TO FIND CRITICAL OX REAL PART AND FREQUENCY AT THE OPERATING FJEL
C PRESSURE DROP RATIO. THE RESULT IS STORED. THE THROTTLING CASE
C (JJ=0) CALLS FOR WRITING OUT SOLUTIONS.
59  IF ((JJ.EQ.1).AND.(IM.EQ.1)) GO TO 60
    IF ((JJ.EQ.1).AND.(IM.EQ.2)) GO TO 62
    IF ((JJ.EQ.1).AND.(IM.EQ.3)) GO TO 64

```

```

GO TO 68
60 IF ((DPF.LT.UPL(1)).OR.(DPF.GT.UPL(N1))) GO TO 79
LI=LI+1
NS=N1-1
DO 61 L=1,NS
IF (DPF.GT.UPL(L+1)) GO TO 61
ACCL(LI)=ACRL(L)+(DPF-UPL(L))*(ACRL(L+1)-ACRL(L))/(UPL(L+1)-UPL(L))
1)
FFI(LI)=FL(L)+(DPF-UPL(L))*(FL(L+1)-FL(L))/(UPL(L+1)-UPL(L))
UPPL(LI)=DPF
GO TO 79
61 CONTINUE
LI=LI-1
GO TO 79
62 IF ((DPF.LT.UPH(1)).OR.(DPF.GT.UPH(N2))) GO TO 79
IL=IL+1
NS=N2-1
DO 63 L=1,NS
IF (DPF.GT.UPH(L+1)) GO TO 63
ACCH(IL)=ACRH(L)+(DPF-UPH(L))*(ACRH(L+1)-ACRH(L))/(UPH(L+1)-UPH(L))
1)
FFH(IL)=FH(L)+(DPF-UPH(L))*(FH(L+1)-FH(L))/(UPH(L+1)-UPH(L))
JPPH(IL)=DPF
GO TO 79
63 CONTINUE
IL=IL-1
GO TO 79
64 IF ((DPF.LT.UPL(1)).OR.(DPF.GT.UPL(N1))) GO TO 66
LI=LI+1
NS=N1-1
DO 65 L=1,NS
IF (DPF.GT.UPL(L+1)) GO TO 65
ACCL(LI)=ACRL(L)+(DPF-UPL(L))*(ACRL(L+1)-ACRL(L))/(UPL(L+1)-UPL(L))
1)
FFL(LI)=FL(L)+(DPF-UPL(L))*(FL(L+1)-FL(L))/(UPL(L+1)-UPL(L))
UPPL(LI)=DPF
GO TO 66
65 CONTINUE
LI=LI-1
GO TO 79
66 IF ((DPF.LT.UPH(1)).OR.(DPF.GT.UPH(N2))) GO TO 79
IL=IL+1
NS=N2-1
DO 67 LJ=1,NS
IF (DPF.GT.UPH(LJ+1)) GO TO 67
ACCH(IL)=ACRH(LJ)+(DPF-UPH(LJ))*(ACRH(LJ+1)-ACRH(LJ))/(UPH(LJ+1)-UPH(LJ))
1)
FFH(IL)=FH(LJ)+(DPF-UPH(LJ))*(FH(LJ+1)-FH(LJ))/(UPH(LJ+1)-UPH(LJ))
UPPH(IL)=DPF
GO TO 79
67 CONTINUE
IL=IL-1
GO TO 79
C AT THIS POINT WRITE OUT ORDERED SOLUTIONS
68 IF (IM.EQ.3) GO TO 72
WRITE (6,69)
69 FORMAT (6X,9HFREQUENCY,9X,14HDELTAP FUEL/PC,6X,12HDELTAP JX/PC)
IF (IM.EQ.2) GO TO 71
WRITE (6,70) (FL(KL),UPL(KL),ACRL(KL),KL=1,N1)
70 FORMAT (8X,0PF5.1,2X,1P2E20.3)

```

```

      GO TO 78
71  WRITE (6,70) (FH(KL),UPH(KL),ACRH(KL),KL=1,N2)
      GO TO 78
72  WRITE (6,73)
73  FORMAT (6X,9HFREQUENCY,9X,14HDELTAP FUEL/PC,6X,12HDELTAP OX/PC,7X,
19HFREQUENCY,7X,14HDELTAP FUEL/PC,7X,12HDELTAP OX/PC)
      ND=N1
      IF (N1.GT.N2) ND=N2
      WRITE (6,74) (FL(KL),UPL(KL),ACRL(KL),FH(KL),UPH(KL),ACRH(KL),KL=1,
1,ND)
74  FORMAT (8X,0PF5.1,2X,1P2E20.3,9X,0PF5.1,2X,1P2E20.3)
      IF (N1-N2) 75,78,77
75  NF=N1+1
      WRITE (6,76) (FH(KL),UPH(KL),ACRH(KL),KL=NE,N2)
76  FORMAT (64X,0PF5.1,2X,1P2E20.3)
      GO TO 78
77  NE=N2+1
      WRITE (6,70) (FL(KL),UPL(KL),ACRL(KL),KL=NE,N1)
C AT THIS POINT, VARIABLE AREA VALUES ARE SPECIFIED
78  IF (JJ.EQ.0) GO TO 88
79  J=2
      K=K+1
      YY=K
      IF (YY.GT.8.) GO TO 80
      IF (YY.EQ.1.) GO TO 87
      APF=APF*YY/(YY-1.)
      EFF1=EFF
      GO TO 14
C AT THIS POINT, THE VARIABLE AREA VALUES OF CRITICAL OX REAL PART
C AND FREQUENCY AT OPERATING FUEL PRESSURE DROP RATIOS ARE
C CONVERTED TO PROPER VARIABLES FOR ORDERING AND WRITING
80  IF ((IL.EQ.0).AND.(LI.EQ.0)) GO TO 89
      IF (IL.EQ.0) GO TO 83
      IF (LI.EQ.0) GO TO 85
      DO 81 IZ=1,LI
      UPL(I7)=UPPL(IZ)
      ACRL(I7)=ACCL(IZ)
      FL(I7)=FFL(IZ)
81  CONTINUE
      N1=LI
      IM=3
      JJ=0
      DO 82 IZ=1,IL
      UPH(I7)=UPPH(IZ)
      ACRH(IZ)=ACCH(IZ)
      FH(IZ)=FFH(IZ)
82  CONTINUE
      N2=IL
      GO TO 53
83  DO 84 IZ=1,LI
      UPL(I7)=UPPL(IZ)
      ACRL(IZ)=ACCL(IZ)
      FL(IZ)=FFL(IZ)
84  CONTINUE
      N1=LI
      IM=1
      JJ=0
      GO TO 53

```

```

85   DO 86 I7=1,IL
      UPH(I7)=UPPH(IZ)
      ACRH(IZ)=ACCH(IZ)
      FH(IZ)=FFH(IZ)
86   CONTINUE
      N2=IL
      IM=2
      JJ=0
      GO TO 56
87   APF=.25*APF
      GO TO 14
88   J=2
89   CONTINUE
      STOP
      END

```

### SUBPROGRAM PVELG

```

C THE FOLLOWING FUNCTION FITS PRIEMS PERCENT VAP VS. ELGEN CURVE
  FUNCTION PP (ELGEE)
  DIMENSION S(17), V(17)
  DATA S(1)/.3/,S(2)/1.0/,S(3)/1.73/,S(4)/2.55/,S(5)/3.42/,S(6)/4.60
  1/,S(7)/6.80/,S(8)/8.00/,S(9)/8.80/,S(10)/12.20/,S(11)/15.80/,S(12)
  2/18.10/,S(13)/24.00/,S(14)/27.00/,S(15)/32.00/,S(16)/35.00/,S(17)/
  340.00/
  DATA V(1)/.1/,V(2)/.26/,V(3)/.38/,V(4)/.48/,V(5)/.56/,V(6)/.64/,V(
  17)/.74/,V(8)/.78/,V(9)/.80/,V(10)/.87/,V(11)/.91/,V(12)/.93/,V(13)
  2/.96/,V(14)/.97/,V(15)/.98/,V(16)/.986/,V(17)/.99/
  DO 1 I=1,16
    IF ((S(I).LE.ELGEE).AND.(ELGEE.LT.S(I+1))) GO TO 2
1  CONTINUE
2  PP=V(I)+(ELGEE-S(I))*(V(I+1)-V(I))/(S(I+1)-S(I))
    IF (PP.GT..99) PP=.99
    RETURN
  END

```

### SUBPROGRAM TMC

```

C THIS MAP FITS THE EMPIRICAL MIXING TIME CURVE
  FUNCTION TM (COEFF)
  DIMENSION S(6), V(6)
  DATA S(1)/.5/,S(2)/1.0/,S(3)/1.5/,S(4)/1.8/,S(5)/2.0/,S(6)/2.2/
  DATA V(1)/.15/,V(2)/.35/,V(3)/.7/,V(4)/1.075/,V(5)/1.4/,V(6)/1.9/
  DO 1 I=1,5
    IF ((S(I).LE.COEFF).AND.(COEFF.LT.S(I+1))) GO TO 2
1  CONTINUE
2  TM=1.-3*(V(I)+(COEFF-S(I))*(V(I+1)-V(I))/(S(I+1)-S(I)))
    RETURN
  END

```

## SUBROUTINE CSTRR

C THE FOLLOWING SUBROUTINE COMPUTES C\* FROM MCBRIDE DATA FOR SELECTED  
C PROPELLANT COMBINATION WITH FUEL AT DESIGN POINT TEMPERATURE

```

SUBROUTINE CSTRR (PCT,DF,CSTAA,SLOPE)
  DIMENSION V(2,7), CS(2), SS(2)
  DATA V(1,1)/6992./,V(1,2)/7072./,V(1,3)/7153./,V(1,4)/7152./,V(1,5
1)/7151./,V(1,6)/7042./,V(1,7)/6934./
  DATA V(2,1)/7027./,V(2,2)/7111./,V(2,3)/7195./,V(2,4)/7196./,V(2,5
1)/7198./,V(2,6)/7086./,V(2,7)/6973./
  IN=DF/.5
  J=IN-7
  Y=5*IN
  Z=.1*Y
  DO 1 I=1,2
  CS(I)=V(I,J)+(V(I,J+1)-V(I,J))*(DF-Z)/.5
  SS(I)=(V(I,J+1)-V(I,J))/.5
1 CONTINUE
  CSTAA=CS(1)+(CS(2)-CS(1))*(PCT-500.)/300.
  SLOPE=SS(1)+(SS(2)-SS(1))*(PCT-500.)/300.
  RETURN
  END

```

## SUBROUTINE RESXP

C THE FOLLOWING SUBROUTINE COMPUTES FLOX PUMP RESISTANCE

```

SUBROUTINE RESXP (C1,C2,RHO,W0,PS,PO,SPEED,RESUP)
  DIMENSION V(10)
  DATA V(1)/.6/,V(2)/.61/,V(3)/.595/,V(4)/.57/,V(5)/.53/,V(6)/.47/,V
1(7)/.4/,V(8)/.31/,V(9)/.21/,V(10)/.095/
  DEPP=PO-PS
  CHN2=DEPP/C2/RHO/1728.*144.
  PHN=448.86*C1/RHO*W0/1728.
  CHPH2=CHN2/(PHN)**2
  DO 5 I=2,10
  Z=I
  F=V(I)-CHPH2*((Z-1.)*.02)**2
  IF (F.GT.0.) GO TO 5
  IF (ABS(F).LE..001) GO TO 3
  PN=(Z-1.)*.02
  PP=(Z-2.)*.02
  VN=V(I)
  VP=V(I-1)
  S=(VN-VP)/.02
1 PG=PP+.5*(PN-PP)
  VG=VP+(PG-PP)*S
  F=VG-CHPH2*PG**2
  IF (ABS(F).LE..001) GO TO 4
  IF (F.GT.0.) GO TO 2
  PN=PG
  VN=VG
  GO TO 1
2 PP=PG

```

```

VP=VG
GO TO 1
3 CHI=CHPH2*((Z-1)*.02)**2
PHI=(Z-1)*.02
S=(V(I)-V(I-1))/.02
GO TO 6
4 CHI=CHPH2*PG**2
PHI=PG
GO TO 6
5 CONTINUE
6 SPEED=448.86*C1/RHO/1728.*W0/PHI
RESOP=-C1*C2*SPEED*3.117*S
RETURN
END

```

## PRINTOUT OF RESULTS FOR DUAL-ORIFICE CONFIGURATION - EFFECT OF FUEL AREA ON STABILITY LIMITS AT FULL THRUST

GAM(1) TK(1) WT(1) GAM(2) TK(2) WT(2)																
1.1691 4537. 19.015 1.1646 4444. 18.900																
PC	ED	NE	NU	F/E	DU	AF/E	C*	L*	EFF	W0	WF	V0	PS	MC	PCI	T4ETAG
500.0	3.	68.	68.	73.5	.0846	.1054E-01	7152.5	40.0	.965	10.46	1.99	508.6	40.0	.149	506.3	3.374E-04
PII	PF	DPF	DPD	L50	LEF	LGEN	PV	TAJT	FTEMP	MJR	DP	TAUM	JS	FTAM		
631.3	654.9	0.2571	.1001	0.769	24.4	55.4	.990	2.132E-03	1344.	3.197	.0140	6.197E-04	.0920	.973		
W0P	W0P/W0	ADJ	UXGAIN	FUELGAIN	SPEEDOX	OXINJDPR	OXSP_ITDPR	OXPMMPRES	OXINJND	OXSCAP	OXMCAIP					
1.056	0.1010	0.2150	40.589	41.033	2.396E 04	5.003E 01	7.492E 01	3.225E 01	6.771E-03	3.431E-05	1.441E-05					
500.0	3.	68.	68.	73.5	.0846	.2634E-02	7152.5	40.0	.965	10.46	1.99	508.6	40.0	.149	506.3	3.374E-04
PII	PF	DPF	DPD	L50	LEF	LGEN	PV	TAJT	FTEMP	MJR	DP	TAUM	JS	FTAM		
631.3	1738.7	2.4609	.1001	0.282	66.8	51.3	.990	1.212E-03	1344.	12.789	.0140	6.584E-04	.0920	.973		
W0P	W0P/W0	ADJ	UXGAIN	FUELGAIN	SPEEDOX	OXINJDPR	OXSP_ITDPR	OXPMMPRES	OXINJND	OXSCAP	OXMCAIP					
1.056	0.1010	0.2150	40.589	41.033	2.396E 04	5.003E 01	7.492E 01	3.225E 01	6.771E-03	3.431E-05	1.441E-05					
500.0	3.	68.	68.	73.5	.0846	.5268E-02	7152.5	40.0	.965	10.46	1.99	508.6	40.0	.149	506.3	3.374E-04
PII	PF	DPF	DPD	L50	LEF	LGEN	PV	TAJT	FTEMP	MJR	DP	TAUM	JS	FTAM		
631.3	977.8	0.9330	.1001	0.465	40.4	91.5	.990	1.553E-03	1344.	6.394	.0140	6.438E-04	.0920	.973		
W0P	W0P/W0	ADJ	UXGAIN	FUELGAIN	SPEEDOX	OXINJDPR	OXSP_ITDPR	OXPMMPRES	OXINJND	OXSCAP	OXMCAIP					
1.056	0.1010	0.2150	40.589	41.033	2.396E 04	5.003E 01	7.492E 01	3.225E 01	6.771E-03	3.431E-05	1.441E-05					
500.0	3.	68.	68.	73.5	.0846	.7901E-02	7152.5	40.0	.965	10.46	1.99	508.6	40.0	.149	506.3	3.374E-04
PII	PF	DPF	DPD	L50	LEF	LGEN	PV	TAJT	FTEMP	MJR	DP	TAUM	JS	FTAM		
631.3	750.3	0.4881	.1001	0.624	30.1	68.2	.990	1.859E-03	1344.	4.263	.0140	6.312E-04	.0920	.973		
W0P	W0P/W0	ADJ	UXGAIN	FUELGAIN	SPEEDOX	OXINJDPR	OXSP_ITDPR	OXPMMPRES	OXINJND	OXSCAP	OXMCAIP					
1.056	0.1010	0.2150	40.589	41.033	2.396E 04	5.003E 01	7.492E 01	3.225E 01	6.771E-03	3.431E-05	1.441E-05					
500.0	3.	68.	68.	73.5	.0846	.1053E-01	7152.5	40.0	.965	10.46	1.99	508.6	40.0	.149	506.3	3.374E-04
PII	PF	DPF	DPD	L50	LEF	LGEN	PV	TAJT	FTEMP	MJR	DP	TAUM	JS	FTAM		
631.3	654.9	0.2571	.1001	0.769	24.4	55.4	.990	2.132E-03	1344.	3.197	.0140	6.197E-04	.0920	.973		
W0P	W0P/W0	ADJ	UXGAIN	FUELGAIN	SPEEDOX	OXINJDPR	OXSP_ITDPR	OXPMMPRES	OXINJND	OXSCAP	OXMCAIP					
1.056	0.1010	0.2150	40.589	41.033	2.396E 04	5.003E 01	7.492E 01	3.225E 01	6.771E-03	3.431E-05	1.441E-05					
500.0	3.	68.	68.	73.5	.0846	.1317E-01	7152.5	40.0	.965	10.46	1.99	508.6	40.0	.149	506.3	3.374E-04
PII	PF	DPF	DPD	L50	LEF	LGEN	PV	TAJT	FTEMP	MJR	DP	TAUM	JS	FTAM		
631.3	609.6	0.1986	.1001	0.904	20.8	47.1	.990	2.387E-03	1344.	2.558	.0140	6.090E-04	.0920	.973		
W0P	W0P/W0	ADJ	UXGAIN	FUELGAIN	SPEEDOX	OXINJDPR	OXSP_ITDPR	OXPMMPRES	OXINJND	OXSCAP	OXMCAIP					
1.056	0.1010	0.2150	40.589	41.033	2.396E 04	5.003E 01	7.492E 01	3.225E 01	6.771E-03	3.431E-05	1.441E-05					
500.0	3.	68.	68.	73.5	.0846	.1580E-01	7152.5	40.0	.965	10.46	1.99	508.6	40.0	.149	506.3	3.374E-04
PII	PF	DPF	DPD	L50	LEF	LGEN	PV	TAJT	FTEMP	MJR	DP	TAUM	JS	FTAM		
631.3	577.1	0.1415	.1001	1.032	18.2	41.3	.990	2.624E-03	1344.	2.131	.0140	5.983E-04	.0920	.973		
W0P	W0P/W0	ADJ	UXGAIN	FUELGAIN	SPEEDOX	OXINJDPR	OXSP_ITDPR	OXPMMPRES	OXINJND	OXSCAP	OXMCAIP					
1.056	0.1010	0.2150	40.589	41.033	2.396E 04	5.003E 01	7.492E 01	3.225E 01	6.771E-03	3.431E-05	1.441E-05					
500.0	3.	68.	68.	73.5	.0846	.1844E-01	7152.5	40.0	.965	10.46	2.00	509.7	40.0	.149	506.3	3.374E-04
PII	PF	DPF	DPD	L50	LEF	LGEN	PV	TAJT	FTEMP	MJR	DP	TAUM	JS	FTAM		
631.8	559.4	0.1061	.1005	1.156	16.3	36.8	.987	2.857E-03	1344.	1.827	.0140	5.891E-04	.0920	.973		
W0P	W0P/W0	ADJ	UXGAIN	FUELGAIN	SPEEDOX	OXINJDPR	OXSP_ITDPR	OXPMMPRES	OXINJND	OXSCAP	OXMCAIP					
1.056	0.1010	0.2150	40.502	40.946	2.397E 04	5.024E 01	7.524E 01	3.227E 01	6.771E-03	3.431E-05	1.441E-05					

PC	ED	NF	NO	F/E	DD	AF/E	C*	L*	EFF	AD	WF	VO	PS	MC	PCI	T-ETAG
500.0	3.	68.	6E.	73.5	.0846	.2107E-01	7152.5	40.0	.959	10.52	2.00	511.7	40.0	.149	305.3	3.335E-04
PII	PF	JPF	UPG	L50	LEF	LGEN	PV	TAJF	FTEMP	MOR	DP	TAJM		JS	ETAM	
032.8	547.7	0.0828	.1013	1.277	14.7	33.3	.983	3.075E-03	1344.	1.599	.0140	5.795E-04		.0920	.373	
WOP	WUP/WUJ	ADV	OXGAIN	FUELGAIN	SPEEDOX	OXINJDPR	JXSP	ITQPR	JXJMPRES	OXINJIND	JXSCAP	JXMCAP				
1.062	0.1010	0.2150	40.338	40.780	2.402E 04	5.063E 01	7.583E 01	3.234E 01	6.771E-03	3.431E-03	1.441E-03					

FREQUENCY	DELTA FUEL/PC	DELTA OX/PC	FREQUENCY	DELTA FUEL/PC	DELTA OX/PC
152.9	8.281E-02	2.389E-02	411.6	8.281E-02	4.499E-02
162.5	1.061E-01	3.156E-02	434.7	1.061E-01	3.465E-02
174.1	1.415E-01	3.990E-02	451.0	1.415E-01	1.921E-02
188.2	1.986E-01	4.927E-02			
205.2	2.971E-01	6.058E-02			
226.5	4.861E-01	7.369E-02			
254.1	9.330E-01	8.509E-02			
296.0	2.461E 00	8.656E-02			

# APPENDIX F

## PROGRAM USERS GUIDE

### Existing Program

A general description of the digital stability program was given in the text. The purpose of this appendix is to describe, in more detail, the structure and operation of the program. This appendix, together with the symbol list in appendix D and the computer listings in appendix E, should serve as a guide in the use of the program. It should be noted that the existing program uses only U. S. customary units. The use of the gravitational conversion factor  $g_c$  is intended to simplify the conversion of the program to the International System (SI) of units.

The program consists of a MAIN program, a curve-fit subprogram PVELG for computing the fraction of oxidizer vaporized within a generalized length (ref. 8), a curve-fit subprogram TMC for computing the gas-phase mixing delay (see fig. 3), a subroutine CSTRR for computing the characteristic velocity and its partial derivative with respect to mixture ratio, and a subroutine RESXP for computing the required pump speed and pump resistance to satisfy the operating values of pump flow rate and pressure rise.

The MAIN program, in conjunction with the other subprograms and subroutines, carries out the required steady-state and stability limit calculations. Figure 14 shows a flow chart of the MAIN program. Statement numbers on the flow chart refer to corresponding statements found in the listing (appendix E).

For the propellants and operating conditions considered in the example, the sensitivity of the specific heat ratio, molecular weight, and combustion temperature in the chamber to the mixture ratio is small. For this reason, values at the nominal mixture ratio are read in as data for two values of chamber pressure (500 and 800 psia) using a format described in statement 1. Linear interpolation is used in the MAIN program to compute these variables at throttled conditions.

For the assumption of a gaseous fuel, supplied from a choked turbine and bypass valve, only the fuel injection temperature and gas constant are required as input fuel properties. For the oxidizer, the density, bulk modulus, viscosity, critical temperature, etc., are required.

Depending on the configuration to be studied, a set of operating conditions (full thrust chamber pressure, mixture ratio, flows) are read into the program. For the example, an index MM was used to identify the type of injector and associated conditions.

The next step in the program is the selection of the type of study to be performed, that is, either throttling with a particular injector ( $JJ = 0$ ) or varying the injector geom-

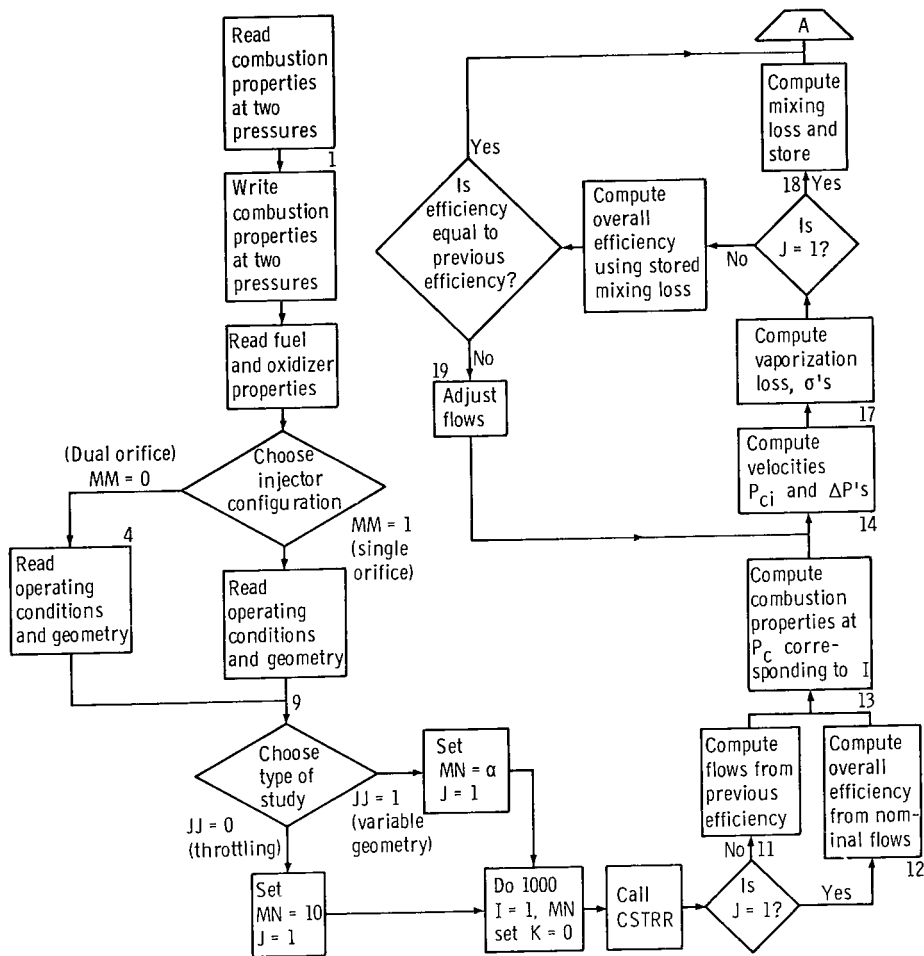


Figure 14. - Flow chart for main program.

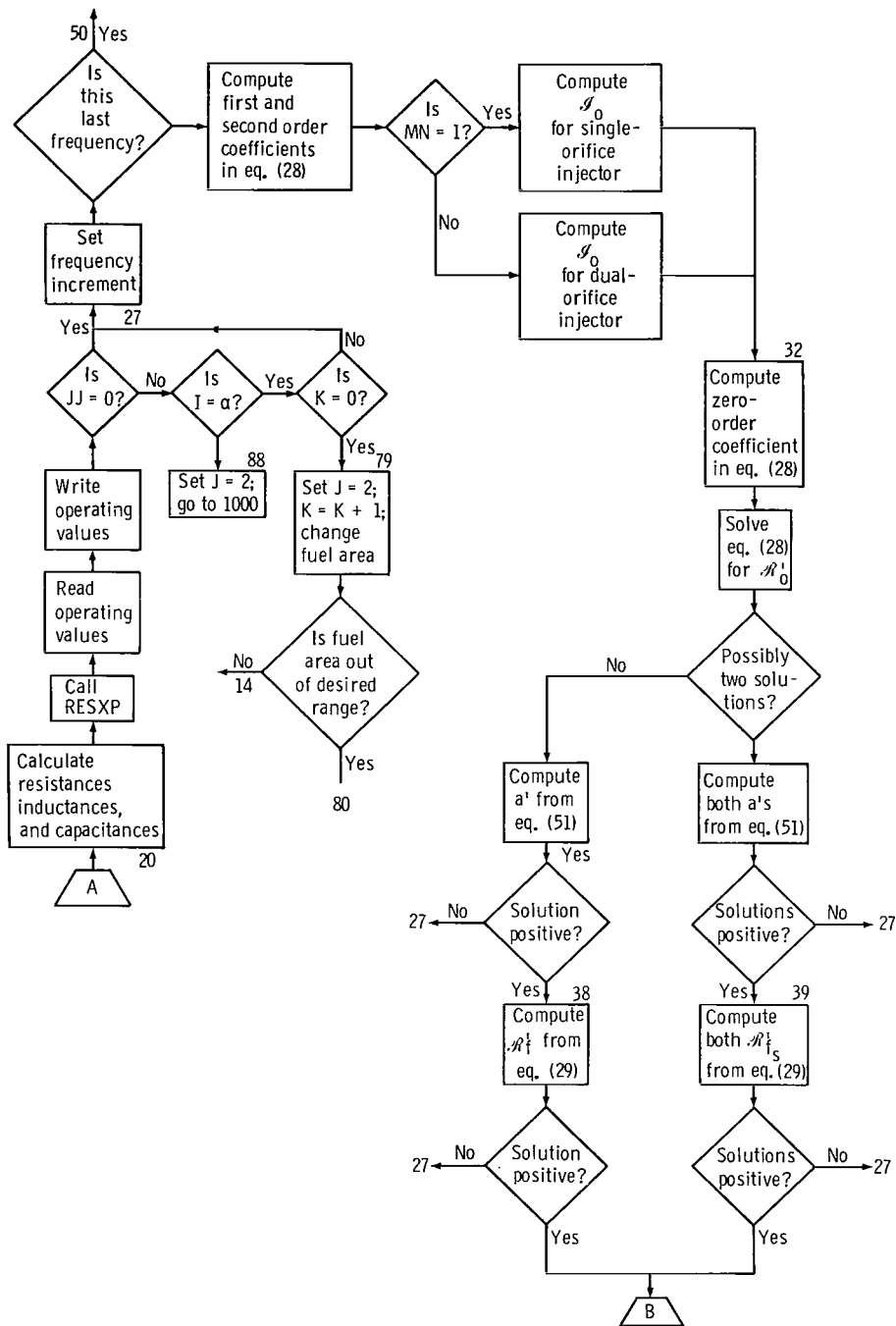


Figure 14. - Continued.

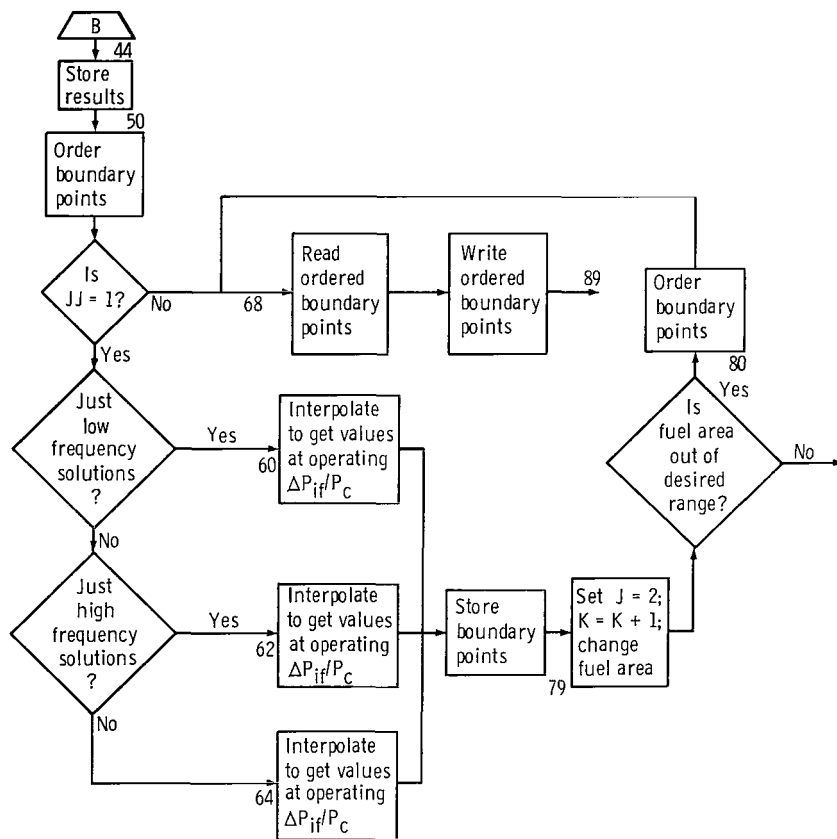


Figure 14. - Concluded.

etry (fuel area in the example) at fixed thrust conditions (JJ = 1).

For varying injector geometry, the existing program must throttle down from full thrust to the desired thrust level before calculating the stability limits.

For each specified chamber pressure at the desired mixture ratio, the subroutine CSTRR is called upon to compute the theoretical  $c^*$ . For the full-thrust nominal-geometry case, the combustion efficiency is computed from the specified chamber pressure and flows, together with the calculated  $c^*$ . For off-design conditions, a previously calculated efficiency is used to compute the flow rates.

Using the calculated values of specific heat ratio, temperature, and molecular weight, the chamber pressure at the injector face is computed from the specified value at the throat. The injector face pressure allows one to calculate the injection velocities, vaporization time delay, and performance loss due to incomplete vaporization (statements 14 and 17). For the full-thrust, nominal geometry case, a performance loss due to incomplete mixing is inferred from the specified overall efficiency and the calculated vaporization loss. For off-design conditions, the mixing loss is assumed equal to the full-thrust value and the overall efficiency is computed and compared with the previously assumed value. If an error exists, the flows are readjusted and the velocities, vaporization time delay, and performance loss due to incomplete vaporization, are recomputed. A suitable mixing model, if available, could be inserted into the program to compute the mixing loss and overall efficiency for all operating conditions.

System pressure drops are then computed. For the dual-orifice case, the secondary (axial) restriction size is adjusted at reduced thrust levels to give a flow split that satisfies a specified vortex characteristic. For the example studied, the characteristic used was fit by the following equation:

$$\frac{\dot{w}_{\text{sec}}}{\dot{w}_o} = \left( \frac{P_{\text{opd}}}{P_{\text{sec}}} \right)^2 + 4.52 \frac{P_{\text{opd}}}{P_{\text{sec}}} - 1.1259 \quad (\text{F1})$$

Linearized resistances, inductances, and capacitances are then calculated at each operating point (statement 20). The subroutine RESXP is called to compute the required pump speed and pump resistance. The pump characteristic ( $\psi_p$  as a function of  $\varphi_p$ ) must be supplied by the user. For the example, values of  $\psi_p$  (CHI) were read in for a range of  $\varphi_p$  (PHI), from 0 to 0.18 in steps of 0.02. The subroutine RESXP uses linear interpolation to determine the speed required to satisfy the operating values of flow, discharge pressure, and inlet pressure. At this point, the operating point values are written out (see appendix E).

For the case of throttling at constant fuel injector area (JJ = 0), the next step is the assumption of a chugging frequency or range of frequencies to be investigated (state-

ment 27). Experience has shown that a lower frequency band extending from about  $3.5/\tau$  Hz (where  $\tau$  is the sum of the oxidizer vaporization time, gas-phase mixing delay and the gas-residence time in ms.) to about  $4.0/\tau$  hertz and a higher frequency band extending from about  $8.7/\tau$  to  $12.0/\tau$  hertz will generally enclose the solutions of interest. Depending on the configuration and operating conditions, solutions in either or both bands may be found. For the examples studied, the solutions occurred at frequencies quite close together. For this reason, a frequency increment of 0.1 hertz was selected in both frequency bands.

At the selected frequency, the coefficients of the second-order equation (28) are calculated. First, the first- and second-order coefficients are determined. Then, the computer evaluates the real and imaginary parts of the oxidizer feed system impedance (appendix C). Using the imaginary part, the zero-order coefficient is computed (statement 32). Equation (28) is then solved for the critical values of the real part of the oxidizer feed-system impedance. If the solution(s) result in a negative value for the injection orifice resistance, frequency is incremented and the calculations are repeated. For positive, real values of the oxidizer injection-orifice resistance  $a'$ , the corresponding values of the fuel-injector resistance  $\mathcal{R}'_f$  are calculating using equation (29). Again, only positive, real values are of interest.

At each frequency where acceptable values of  $a'$  and  $\mathcal{R}'_f$  are found, the resistances are converted to critical pressure drop to chamber pressure ratios  $(\overline{\Delta P}_{io}/\overline{P}_c)'$  and  $(\overline{\Delta P}_{if}/\overline{P}_c)'$  using equations (57) and (58). These values, together with frequency, are stored (statement 44). After the desired range(s) of frequency are covered, the stored sets of values are sorted in order of increasing values of  $(\overline{\Delta P}_{if}/\overline{P}_c)'$  (statement 147). This choice is based on experience with these configurations where boundaries may have double values of  $(\overline{\Delta P}_{if}/\overline{P}_c)'$  for a selected value of  $(\overline{\Delta P}_{io}/\overline{P}_c)'$ . The ordering of points makes it possible to use existing computer plot routines and also makes it easier to read the computer output (see appendix E). At this point, the sets of points are written out (statement 68). The procedure is then repeated at the lower thrust levels.

A similar procedure is followed for the fixed-thrust, variable fuel area case. However, the dynamic portion of the program is not used until the system is throttled down from full-thrust conditions to the desired  $\overline{P}_c$  level. The dynamic portion of the program is then run at the desired  $\overline{P}_c$  and the specified mixture ratio. For the nominal fuel area, a set of boundary points is obtained in either the low-frequency range (statement 60), the high-frequency range (statement 62), or both (statement 64). Since the solutions are obtained using the delay values corresponding to the operating value of  $\overline{\Delta P}_{if}/\overline{P}_c$ , interpolation is used to determine both the frequency and  $(\overline{\Delta P}_{io}/\overline{P}_c)'$  corresponding to  $(\overline{\Delta P}_{if}/\overline{P}_c)' = \overline{\Delta P}_{if}/\overline{P}_c$ . This set of points is then stored. The fuel area is then changed and the procedure is repeated. After the desired range of areas has been

covered, the resulting sets of points are sorted in order of increasing  $(\overline{\Delta P_{if}}/\overline{P_c})'$  (see statement 80). The results are then written out (statement 68).

## Modification of Existing Program

The digital program, as described previously, is set up for a gaseous methane, liquid-flox propellant combination operating in an expander type cycle. The program is, however, capable of generating stability limits for any propellant combination or engine configuration desired. The following section is intended as a guide in changing the existing program to serve one's individual needs.

Changes in the propellant combination can be conveniently handled if the required input data are available. For other gaseous-fuel liquid-oxidizer combinations, changes in the fuel gas constant, fuel-injection temperature schedule, oxidizer properties, and combustion properties are required. The case of a liquid-liquid propellant combination can be handled if the following points are considered:

- (1) All input data now supplied for the oxidizer are supplied for both propellants.
- (2) Two pump characteristics are supplied with their corresponding subroutines for speed and resistance calculations.
- (3) Both feed systems are represented by impedance which are made up of resistances, inductances, and capacitances. This representation will probably result in a more complicated form for the real and imaginary parts of the fuel feed-system impedance. Transformation of the critical values of the real part to pressure drop ratios will involve subtraction of frequency-sensitive terms as is now done with the oxidizer.
- (4) Drop sizes must be computed for both propellants. Constant drop sizes, based on injector geometry (ref. 8), or other suitable correlations must be used.
- (5) Computation of effective lengths, vaporization time delays, percent vaporized, etc., must be made for both propellants; this will require double useage of the generalized length-percent vaporized curve.
- (6) Computation of the vaporization efficiency (ETAV) must be made using equation (52) in reference 8. In this report, equation (53) in reference 8 is used for the case of a completely vaporized fuel.
- (7) The solution of the characteristic equation and the generation of stability limits can be accomplished by redefining the following terms:  $THETAM = W * (TAUM + TAUV0)$ ,  $THETAV = W * (TAUV0 - TAUVF)$ , and  $THETAT = W * (TAUM + TAUV0)$  where TAUV0 and TAUVF are the oxidizer and fuel vaporization times, respectively. TAUM is the gas-phase delay as previously defined. The vaporization delays must be computed separately.

Different feed-system configurations (valves, orifices, lines, etc.) require changes in the section used to compute the real and imaginary parts of the feed-system impedances. In addition, the steady-state pressure-drop calculations must be adjusted. For the impedance calculations, the techniques described in appendix C should be used to set up the reduction equations in the program.

## REFERENCES

1. Wenzel, Leon M.; and Szuch, John R.: Analysis of Chugging in Liquid-Bipropellant Rocket Engines Using Propellants with Different Vaporization Rates. NASA TN D-3080, 1965.
2. Szuch, John R.; and Wenzel, Leon M.: Experimental Verification of a Double Dead-Time Model Describing Chugging in Liquid Bipropellant Rocket Engines. NASA TN D-4564, 1968.
3. Szuch, John R.: Application of a Double-Dead-Time Model Describing Chugging to Liquid-Propellant Rocket Engines Having Multielement Injectors. NASA TN D-5303, 1969.
4. Heidmann, Marcus F.; Sokolowski, Daniel E.; and Diehl, Lawrence A.: Study of Chugging Instability with Liquid-Oxygen and Gaseous-Hydrogen Combustors. NASA TN D-4005, 1967.
5. Anon.: J-2 Program Quarterly Progress Report for Period Ending February 28, 1962. Rep. R-2600-6, Rocketdyne Div., North American Aviation, (NASA CR-63323), Mar. 28, 1962, pp. 85, 137-140.
6. Heidmann, Marcus F.: Oxygen-Jet Behavior During Combustion Instability in a Two-Dimensional Combustor. NASA TN D-2725, 1965.
7. Dankoff, Walter F.; Johnsen, Irving A.; Conrad, E. William; and Tomazic, William A.: M-1 Injector Development - Philosophy and Implementation. NASA TN D-4730, 1968.
8. Priem, Richard J.; and Heidmann, Marcus F.: Propellant Vaporization as a Design Criterion for Rocket Engine Combustion Chambers. NASA TR R-67, 1960.
9. Hersch, Martin; and Rice, Edward J.: Gaseous-Hydrogen-Liquid-Oxygen Rocket Combustion at Supercritical Chamber Pressures. NASA TN D-4172, 1967.
10. Ingebo, Robert D.; and Foster, Hampton H.: Drop-Size Distribution for Crosscurrent Breakup of Liquid Jets in Airstreams. NACA TN 4087, 1957.
11. Hersch, Martin: A Mixing Model for Rocket Engine Combustion. NASA TN D-2881, 1965.
12. Summerfield, Martin: A Theory of Unstable Combustion in Liquid Propellant Rocket Systems. ARS J., vol. 21, no. 5, Sept. 1951, pp. 108-114.
13. Drain, Daniel I.; Schum, Harold J.; and Wasserbauer, Charles A.: Relations of Combustion Dead Time to Engine Variables for a 20,000-Pound-Thrust Gaseous-Hydrogen-Liquid-Oxygen Rocket Engine. NASA TN D-851, 1961.

- 
14. Crocco, Luigi; and Cheng, Sin-I: Theory of Combustion Instability in Liquid Propellant Rocket Motors. AGARDograph No. 8, Butterworths Sci. Pub. , 1956.
  15. Hurrell, Herbert G.: Analysis of Injection-Velocity Effects on Rocket Motor Dynamics and Stability. NASA TR R-43, 1959.
  16. Heidmann, Marcus F.; and Wieber, Paul R.: Analysis of Frequency Response Characteristics of Propellant Vaporization. NASA TN D-3749, 1966.
  17. Van Valkenburg, Mac E.: Network Analysis. Prentice-Hall, Inc. , 1955.
  18. Kasselmann, J. T.; and Rivard, J. G.: Development of an All-Fluid Amplifier for Liquid Rocket Applications. Rep. BC/RLD-3015, Bendix Corp. (NASA CR-54446), Nov. 1965.

FIRST CLASS MAIL



POSTAGE AND FEES PAID  
NATIONAL AERONAUTICS AND  
SPACE ADMINISTRATION

04U 001 53 51 3DS 70348 00903  
AIR FORCE WEAPONS LABORATORY /WLOL/  
KIRTLAND AFB, NEW MEXICO 87117

ATT E. LOU BOWMAN, CHIEF, TECH. LIBRARY

POSTMASTER: If Undeliverable (Section 158  
Postal Manual) Do Not Return

*"The aeronautical and space activities of the United States shall be conducted so as to contribute . . . to the expansion of human knowledge of phenomena in the atmosphere and space. The Administration shall provide for the widest practicable and appropriate dissemination of information concerning its activities and the results thereof."*

— NATIONAL AERONAUTICS AND SPACE ACT OF 1958

## NASA SCIENTIFIC AND TECHNICAL PUBLICATIONS

**TECHNICAL REPORTS:** Scientific and technical information considered important, complete, and a lasting contribution to existing knowledge.

**TECHNICAL NOTES:** Information less broad in scope but nevertheless of importance as a contribution to existing knowledge.

**TECHNICAL MEMORANDUMS:** Information receiving limited distribution because of preliminary data, security classification, or other reasons.

**CONTRACTOR REPORTS:** Scientific and technical information generated under a NASA contract or grant and considered an important contribution to existing knowledge.

**TECHNICAL TRANSLATIONS:** Information published in a foreign language considered to merit NASA distribution in English.

**SPECIAL PUBLICATIONS:** Information derived from or of value to NASA activities. Publications include conference proceedings, monographs, data compilations, handbooks, sourcebooks, and special bibliographies.

**TECHNOLOGY UTILIZATION PUBLICATIONS:** Information on technology used by NASA that may be of particular interest in commercial and other non-aerospace applications. Publications include Tech Briefs, Technology Utilization Reports and Notes, and Technology Surveys.

*Details on the availability of these publications may be obtained from:*

SCIENTIFIC AND TECHNICAL INFORMATION DIVISION  
NATIONAL AERONAUTICS AND SPACE ADMINISTRATION  
Washington, D.C. 20546